UCRL-16372

University of California

Ernest O. Lawrence Radiation Laboratory

TWO-WEEK LOAN COPY

This is a Library Circulating Copy which may be borrowed for two weeks. For a personal retention copy, call Tech. Info. Division, Ext. 5545

MEASUREMENT OF THE VELOCITY OF GASES WITH VARIABLE FLUID PROPERTIES

Berkeley, California

DISCLAIMER

This document was prepared as an account of work sponsored by the United States Government. While this document is believed to contain correct information, neither the United States Government nor any agency thereof, nor the Regents of the University of California, nor any of their employees, makes any warranty, express or implied, or assumes any legal responsibility for the accuracy, completeness, or usefulness of any information, apparatus, product, or process disclosed, or represents that its use would not infringe privately owned rights. Reference herein to any specific commercial product, process, or service by its trade name, trademark, manufacturer, or otherwise, does not necessarily constitute or imply its endorsement, recommendation, or favoring by the United States Government or any agency thereof, or the Regents of the University of California. The views and opinions of authors expressed herein do not necessarily state or reflect those of the United States Government or any agency thereof or the Regents of the University of California.

UCRL-16372

UNIVERSITY OF CALIFORNIA

Lawrence Radiation Laboratory
Berkeley, California

AEC Contract No. W-7405-eng-48

MEASUREMENT OF THE VELOCITY OF GASES WITH VARIABLE FLUID PROPERTIES

D. T. Wasan, R. M. Davis, and C. R. Wilke

August 1965

MEASUREMENT OF THE VELOCITY OF GASES WITH VARIABLE FLUID PROPERTIES*

D. T. Wasan,† R. M. Davis, and C. R. Wilke

Department of Chemical Engineering and Lawrence Radiation Laboratory
University of California
Berkeley, California

August 1965

ABSTRACT

This paper describes the experimental measurements of the time averaged velocities of gases in a field of variable composition and temperature. The conventional theory of hot wire anemometry is extended to include the effects of both natural and forced convection to gases having variable fluid properties. Observations of the fully developed turbulent velocity fields in the presence of moderate mass transfer rates revealed no significant effect of mass transfer on the velocity distribution.

---

*This work was done under the auspices of the U. S. Atomic Energy Commission.

†D. T. Wasan is with the Department of Chemical Engineering, Illinois Institute of Technology, Chicago, Illinois 60616

INTRODUCTION

The effects of injection and suction on the velocity field have been studied extensively from both a theoretical and experimental standpoint for the case of a flat plate (11, 12, 13, 16, 17, 18). Similar studies have also been carried out for the case of a circular cylinder (21) and for channel flow. These analyses indicate that at finite rates of injection (injection is comparable to the evaporation of a liquid into a gas stream), the velocity profile is distorted from its typical shape with no injection. It follows that in order to gain a more fundamental knowledge of the turbulent forced convection-diffusion systems, simultaneous measurements of velocity and concentration profiles should be made within the transfer equipment since the two processes are closely coupled.

In the past, at subsonic flow rates, the hot wire anemometer has been used to measure velocities of gases in a field of constant composition and temperature. For this case, King (8, 9) in his classic papers showed that if a gas stream with constant fluid properties is passed over a heated horizontal wire, the current flowing through the wire may be related to the stream velocity in a manner which may be determined by calibrated tests. However, in a study such as the one at hand, where velocity measurements are to be made in a fluid field of variable composition and temperature, it is essential that the effect on the current-velocity relationship caused by a change in fluid properties be accounted for (2, 3).

The present study is divided into two parts.

In Part I, the general theoretical treatment of hot wire anemometry technique is presented to apply to the measurement of low velocities of gases with nonuniform composition and temperature. Equations are presented from which the time averaged and the fluctuating velocities of gases with variable composition and temperature can be calculated. The validity of the proposed equation for calculating the time averaged velocities was established by velocity measurements.

In Part II, observations of the fully developed turbulent velocity fields in the presence of moderate mass transfer rates are reported.

Part I. HOT WIRE ANEMOMETRY

It is well established (8, 9) that if a gas stream with constant fluid properties is passed over a heated horizontal wire, the current, I flowing through the wire may be related to the stream velocity, u by

$$\frac{I^2 R_w}{t_w - t_a} = \frac{I^2 R_w}{\Delta t} = a + b\sqrt{u} \qquad (1)$$

where R_w is the wire resistance, Δt is the difference between the wire and fluid temperature, and a and b are equation constants whose value depends upon the fluid properties and the wire dimensions. Equation (1) is generally known as King's equation.

From King's equation (Equation (1)) it is evident that if a plot of heat dissipation as given by $(I^2R_w/\Delta t)$ versus $\sqrt{u}$ is made, then the constants a and b can be determined from the intercept and slope of the straight line that best fits the data from calibrated tests with known velocities. It has been found experimentally that in the case of pure forced convection at Reynolds numbers greater than 5.0, the relationship as given by Equation (1) can be represented by a linear function (6). However, Van der Hegge Zijnen's experimental observations (22) of heat transfer to cylinders clearly show that the effect of natural convection becomes important at low velocities. As a result, it is desirable to develop a general equation for hot wire anemometry which will include the low velocity range, and which will also account for the change in properties resulting from the change in composition and temperature. This general development is given in the following section.

A. Generalized Development of the Hot Wire Anemometry Theory

Consider the hot wire anemometer as a horizontal cylinder of infinite length which gives off heat to its surroundings by forced and natural convection as well as by radiation.

The mechanism of heat transfer from a horizontal cylinder by natural or by forced convection has been studied extensively. Van der Hegge Zijnen (22) has collected the heat transfer data for a wide range of systems studied by several experimentors, and has correlated these data successfully as follows. For natural convection

from a horizontal cylinder for the range of product of Grashof (Gr) and Prandtl (Pr) numbers of 10^{-5} to 10^{9}, the Nusselt (Nu) number is given by

$$Nu_n = 0.38(Pr)_f^{0.2} + 0.25[(Gr)_f(Pr)_f]^{1/8} + 0.45[(Gr)_f(Pr)_f]^{1/4} \quad (2)$$

For forced convection from a horizontal cylinder, for the Reynolds (Re) number range of 10^{-2} to 10^{6}, the Nusselt number is given by

$$Nu_{fo} = 0.38(Pr)_f^{0.2} + [0.56(Re)_f^{1/2} + 0.001(Re)_f](Pr)_f^{1/3} \quad (3a)$$

According to Van der Hegge Zijnen, the term containing the Reynolds number to the first power in Equation (3a) may be neglected at low velocities, thus we obtain

$$Nu_{fo} = 0.38(Pr)_f^{0.2} + 0.56(Re)_f^{1/2}(Pr)_f^{1/3} \quad (3b)$$

When a fluid stream flows over a heated cylinder at low velocities, heat is transferred from the wire to the gas by natural as well as by forced convection. The nature of the combination of these two modes of heat transfer is not well understood. The only study of this problem is reported by Van der Hegge Zijnen (22) who has successfully correlated data for air by assuming that the forced and natural convection modes of heat transfer may be represented by horizontal and vertical vectors respectively. The total amount of heat transferred by the cylinder may therefore be expressed by the resultant of the two vectors. Although Van der Hegge Zijnen only

verified the validity of this assumption for air, there is no reason why this assumption should not hold for other systems. By using the assumption of vectorial additivity, Equations (2) and (3b) may be combined as follows,

$$\{Nu_t - 0.38(Pr)_f^{0.20}\}^2 = \{0.25[(Gr)_f(Pr)_f]^{1/8} + 0.45[(Gr)_f(Pr)_f]^{1/4}\}^2 + \{0.56(Re)_f^{1/2}(Pr)_f^{1/3}\}^2 \quad (4)$$

Rearranging terms in the above equation, we get

$$Nu_t = 0.38(Pr)_f^{0.2} + \sqrt{\alpha^2 + \beta^2 u} \quad (5)$$

where

$$\alpha = 0.25[(Gr)_f(Pr)_f]^{1/8} + 0.45[(Gr)_f(Pr)_f]^{1/4} \quad (6)$$

and

$$\beta = 0.56(D\rho_f/\mu_f)^{1/2}(Pr)_f^{1/3} \quad (7)$$

If we make the usual assumptions (6, 8, 10, 19) that the wire heat losses are all to the fluid stream, that the wire is heated to a uniform temperature, and that the heat given off by the wire does not affect the fluid properties of the ambient stream, then we may equate the heat dissipation of the wire to the heat transferred to the gas stream as

$$I^2R_w = \epsilon h_t A\Delta t \quad (8)$$

where h_t is the total heat transfer coefficient which represents natural and forced convection as well as radiation from the wire, A is the surface area of the wire available for heat transfer, and ϵ is an energy conversion factor.

Substituting relation (5) into relation (8) we have

$$\frac{I^2 R_w}{\epsilon A \Delta t} = h_t = h_r + \left(\frac{k_f}{D}\right) \left[0.38 (Pr)_f^{0.2} + \sqrt{\alpha^2 + \beta^2 u}\right] \tag{9}$$

Hinze (6) has shown that if the wire diameter is less than 15 microns, and if the wire temperature does not exceed 300° C (as will be the case in this study), the heat transfer coefficient for radiation, h_r, which appears in Equation (9) may be neglected.

Combining Equations (6), (7), and (9) and after making necessary algebraic rearrangements the velocity can be expressed explicitly as

$$u = \frac{D^2}{\epsilon^2 A^2 k_f^2 \left[0.56 \left(\frac{D\rho_f}{\mu_f}\right)^{1/2} (Pr)_f^{1/3}\right]^2} \left(\left(\frac{I^2 R_w}{\Delta t}\right)^2 - 0.76 \epsilon A \left(\frac{k_f}{D}\right) \left(\frac{I^2 R_w}{\Delta t}\right) (Pr)_f^{0.2} + \left\{0.38 \epsilon A \left(\frac{k_f}{D}\right) (Pr)_f^{0.2}\right\}^2 - \epsilon^2 A^2 \left(\frac{k_f}{D}\right)^2 \left\{0.25 [(Gr)_f (Pr)_f]^{1/8} + 0.45 [(Gr)_f (Pr)_f]^{1/4}\right\}^2 \right) \tag{10}$$

If the two constants K_1 and K_2 may be expressed as

$$K_1 = (\epsilon A)/D = \epsilon \pi L \tag{11}$$

$$K_2 = (0.56\epsilon A)^2/D = (0.56\epsilon\pi L)^2 D \tag{12}$$

then Equation (10) may be rewritten as

$$u = \frac{\left(\frac{I^2 R_w}{\Delta t}\right)^2 - 0.76 k_f \left(\frac{I^2 R_w}{\Delta t}\right)(Pr)_f^{0.2} K_1}{[\rho_f (C_p)_f^{2/3} k_f^{4/3}/\mu_f^{1/3}] K_2} + \frac{k_f^2 \left\{\{0.38(Pr)_f^{0.2}\}^2 - \{0.25[(Gr)_f (Pr)_f]^{1/8} + 0.45[(Gr)_f (Pr)_f]^{1/4}\}^2\right\} K_1^2}{[\rho_f (C_p)_f^{2/3} k_f^{4/3}/\mu_f^{1/3}] K_2} \tag{13}$$

Examination of Equation (13) reveals that the velocity of a gas may be calculated from measured values of the wire resistance, current, temperature, values of the fluid properties evaluated at the mean film temperature and from the known values of the constants K_1 and K_2. It is to be noted that these constants are functions of length and diameter of the wire alone. Since precise measurements of the parameters is difficult, equation constants are generally determined by calibrated tests in a known velocity field. Furthermore, it should be pointed out that the values of K_1 and K_2 determined by calibration in one gas may be used to calculate velocities measured in another gas, since the only variables involved in these constants are length and diameter.

A series of computer (IBM 7094) programs were written to compute the equation constants from calibration data. These programs and the related details are given elsewhere (4).

The above procedure can be extended to obtain an expression for calculating the fluctuating velocity in flowing mixture of gases as follows.

Neglecting the effect of radiation Equation (9) may be written in the following form:

$$\frac{I^2R_w}{\epsilon A\Delta t} = \frac{P}{\epsilon A\Delta t} = \frac{0.38}{D}(C_p\mu k^4)^{1/5} + \left[\frac{0.0625}{D^{3/2}}\left(\frac{C_p\rho^2k^7}{\mu}\right)^{1/4}(gD\beta'\Delta t)^{1/4}\right.$$

$$+ \frac{0.225}{D^{5/4}}\left(\frac{C_p\rho^2K^{13/3}}{\mu}\right)^{3/8}(gD\beta'\Delta t)^{3/8}$$

$$+ \frac{0.202}{D}\left(\frac{C_p\rho^2K^3}{\mu}\right)^{1/2}(gD\beta'\Delta t)^{1/2}$$

$$\left.+ \frac{0.314}{D}\left(\frac{C_p^2K^3\rho^3}{\mu}\right)^{1/3} u\right]^{1/2} \qquad (14)$$

Differentiating the above equation and after making necessary algebraic manupulations we obtain

$$\frac{dP}{\epsilon A\Delta t} = \frac{P'}{\epsilon A\Delta t} = \frac{0.38}{D}\left(\frac{1}{5}\right)\left(C_p\mu K^4\right)^{1/5}\left(\frac{C_p'}{C_p} + \frac{\mu'}{\mu} + \frac{4K'}{K}\right)$$

$$+ \frac{1}{2}\left[\frac{0.0625}{D^{3/2}}\left(\frac{C_p\rho^2K^7}{\mu}\right)^{1/4}(gD\beta'\Delta t)^{1/4} + \frac{0.225}{D^{5/4}}\left(\frac{C_p\rho^2K^{13/3}}{\mu}\right)^{3/8}(gD\beta'\Delta t)^{3/8}\right.$$

$$\left. + \frac{0.202}{D}\left(\frac{C_p\rho^2K^3}{\mu}\right)^{1/2}(gD\beta'\Delta t)^{1/2} + \frac{0.314}{D}\left(\frac{C_p^2K^3\rho^3}{\mu}\right)^{1/3}u\right]^{-1/2}$$

$$\times\left[\frac{0.0625}{D^{3/2}}\left(\frac{1}{4}\right)\left(\frac{C_p\rho^2K^7}{\mu}\right)^{1/4}(gD\beta'\Delta t)^{1/4}\left(\frac{C_p'}{C_p} + \frac{2\rho'}{\rho} + \frac{7K'}{K} - \frac{\mu'}{\mu}\right)\right.$$

$$+ \frac{0.225}{D^{5/4}}\left(\frac{3}{8}\right)\left(\frac{C_p\rho^2K^{13/3}}{\mu}\right)^{3/8}(gD\beta'\Delta t)^{3/8}\left(\frac{C_p'}{C_p} + \frac{2\rho'}{\rho} + \frac{13}{3}\frac{K'}{K} - \frac{\mu'}{\mu}\right)$$

$$+ \frac{0.202}{D}\left(\frac{1}{2}\right)\left(\frac{C_p\rho^2K^3}{\mu}\right)^{1/2}(gD\beta'\Delta t)^{1/2}\left(\frac{C_p'}{C_p} + \frac{2\rho'}{\rho} + \frac{3K'}{K} - \frac{\mu'}{\mu}\right)$$

$$\left. + \frac{0.314}{D}u\left(\frac{1}{3}\right)\left(\frac{C_p^2K^3\rho^3}{\mu}\right)^{1/3}\left(\frac{2C_p'}{C_p} + \frac{3K'}{K} + \frac{3\rho'}{\rho} - \frac{\mu'}{\mu}\right) + \frac{0.314}{D}\left(\frac{C_p^2K^3\rho^3}{\mu}\right)^{1/3}u'\right] \quad (15)$$

In Equation (15) P', K', C_p', μ', ρ', and u' are designated as small fluctions in power, thermal conductivity, specific heat, viscosity, density and fluid velocity defined as follows

$$\begin{aligned} P &= \overline{P} + P' \\ K &= \overline{K} + K' \\ C_p &= \overline{C}_p + C_p' \\ \mu &= \overline{\mu} + \mu' \\ \rho &= \overline{\rho} + \rho' \\ u &= \overline{u} + u' \end{aligned} \quad (16)$$

Also a small fluctuation in gas composition is defined as $x = \bar{x} + x'$. Collecting the coefficients of the fluctuating quantities and after making algebraic simplifications Equation (15) may be written as

$$\frac{P'}{\epsilon A \Delta t} = K' \left[\frac{0.304}{D} \left(\frac{C_p \mu}{K} \right)^{1/5} + \frac{1}{2}(X)^{-1/2} \left\{ \frac{0.1094}{D^{3/2}} \left(\frac{C_p \rho^2 K^3}{\mu} \right)^{1/4} (gD\beta' \Delta t)^{1/4} \right.\right.$$

$$+ \frac{0.3656}{D^{5/4}} \left(\frac{C_p \rho^2 K^{5/3}}{\mu} \right)^{3/8} (gD\beta' \Delta t)^{3/8} + \frac{0.303}{D} \left(\frac{C_p \rho^2 K^3}{\mu} \right)^{1/2} (gD\beta' \Delta t)^{1/2}$$

$$\left.\left. + \frac{0.314}{D} \left(\frac{C_p^2 \rho^3}{\mu} \right)^{1/3} u \right\} \right]$$

$$+ C_p' \frac{0.076}{D} \left(\frac{\mu K^4}{C_p^4} \right)^{1/5} + \frac{1}{2}(X)^{-1/2} \left\{ \frac{0.0156}{D^{3/2}} \left(\frac{\rho^2 K^7}{\mu C_p^3} \right)^{1/4} (gD\beta' \Delta t)^{1/4} \right.$$

$$+ \frac{0.0844}{D^{5/4}} \left(\frac{\rho^2 K^{13/3}}{\mu C_p^{5/3}} \right)^{3/8} (gD\beta' \Delta t)^{3/8} + \frac{0.101}{D} \left(\frac{C_p \rho^2 K^3}{\mu} \right)^{1/2} (gD\beta' \Delta t)^{1/2}$$

$$\left.\left. + \frac{0.2093}{D} \left(\frac{K^3 \rho^3}{\mu C_p} \right)^{1/3} u \right\} \right]$$

$$+ \mu' \left[\frac{0.076}{D} \left(\frac{C_p K^4}{\mu^4} \right)^{1/5} - \frac{1}{2}(X)^{-1/2} \left\{ \frac{0.0156}{D^{3/2}} \left(\frac{C_p \rho^2 K^7}{\mu^5} \right)^{1/4} (gD\beta' \Delta t)^{1/4} \right.\right.$$

$$+ \frac{0.0844}{D^{5/4}} \left(\frac{C_p \rho^2 K^{13/3}}{\mu^{1/3}} \right)^{3/8} (gD\beta' \Delta t)^{3/8} + \frac{0.101}{D} \left(\frac{C_p \rho^2 K^3}{\mu} \right)^{1/2} (gD\beta' \Delta t)^{1/2}$$

$$\left.\left. + \frac{0.105}{D} \left(\frac{C_p^2 K^3 \rho^3}{\mu^4} \right)^{1/3} u \right\} \right]$$

$$+ \rho' \left[\frac{1}{2}(X)^{-1/2} \left\{ \frac{0.0313}{D^{3/2}} \left(\frac{C_p K^7}{\mu \rho^2} \right)^{1/4} (gD\beta'\Delta t)^{1/4} + \frac{0.1688}{D^{5/4}} \left(\frac{C_p K^{13/3}}{\mu \rho^{2/3}} \right)^{3/8} (gD\beta'\Delta t)^{3/8} \right.\right.$$

$$\left.\left. + \frac{0.202}{D} \left(\frac{C_p \rho^2 K^3}{\mu} \right)^{1/2} (gD\beta'\Delta t)^{1/2} + \frac{0.314}{D} \left(\frac{C_p^2 K^3}{\mu} \right)^{1/3} u \right\} \right]$$

$$+ u' \left[\frac{1}{2}(X)^{-1/2} \left\{ \frac{0.314}{D} \left(\frac{C_p^2 K^3 \rho^3}{\mu} \right)^{1/3} \right\} \right] \tag{17}$$

where

$$(X)^{-1/2} = \left[\frac{0.0625}{D^{3/2}} \left(\frac{C_p \rho^2 K^7}{\mu} \right)^{1/4} (gD\beta'\Delta t)^{1/4} \right.$$

$$+ \frac{0.225}{D^{5/4}} \left(\frac{C_p \rho^2 K^{13/3}}{\mu} \right)^{3/8} (gD\beta'\Delta t)^{3/8}$$

$$+ \frac{0.202}{D} \left(\frac{C_p \rho^2 K^3}{\mu} \right)^{1/2} (gD\beta'\Delta t)^{1/2}$$

$$\left. + \frac{0.314}{D} \left(\frac{C_p^2 \rho^3 K^3}{\mu} \right)^{1/3} u \right]^{-1/2}$$

Equation (17) can also be derived by following a procedure different from the one indicated above. This procedure involves substituting relations (16) into Equation (14), using binomial expansions in the fluctuating quantities, neglecting cross product terms in the fluctuating quantities, and subtracting the averaged form of Equation (14) from the final relation to obtain Equation (17). This procedure is quite cumbersome and will not be detailed here. It should also be noted that Equation (17) has been derived for a constant wire temperature operation.

The expressions for the mean density and the mean specific heat at constant pressure of a gas-air mixture are written as the simple weighted average as follows:

$$\bar{\rho} = \rho_a + \bar{x}_g(\rho_a - \rho_g) = \rho_a + \bar{x}\,\Delta\rho \tag{18}$$

$$\bar{C}_p = C_{p_a} + \bar{x}_g(C_{p_a} - C_{p_g}) = C_{p_a} + \bar{x}\,\Delta C_p \tag{19}$$

where $\bar{x}_g$ is the mean mole fraction of the secondary gas in a gas-air mixture.

The expressions for the mean thermal conductivity and the mean viscosity are written as

$$\bar{K} = K_a + F(\bar{x})(K_a - K_g) = K_a + F(\bar{x})\Delta k \tag{20}$$

$$\bar{\mu} = \mu_a + G(\bar{x})(\mu_a - \mu_g) = \mu_a + G(\bar{x})\Delta\mu \tag{21}$$

The thermal conductivity and viscosity of gas mixtures are not a simple weighted average and vary considerably for most of the pairs of gases. However, the function $F(\bar{x})$ can be deduced from the expression recently proposed by Cheung, Bromley, and Wilke (1) for thermal conductivity of gas mixtures. The function $G(\bar{x})$ can be deduced from the relations recommended by Reid and Sherwood (15).

From Equations (18), (19), (20), and (21) we have

$$\rho' = x'\Delta\rho$$

$$C_p' = x'\Delta C_p$$

$$K' = \frac{dF(\bar{x})}{d\bar{x}} x'\Delta k \tag{22}$$

and

$$\mu' = \frac{dG(\bar{x})}{d\bar{x}} x'\Delta\mu$$

Substituting relation (22) into Equation (17) yields

$$\frac{P'}{\epsilon A\Delta t} = x'\Delta k\frac{dF(\bar{x})}{d\bar{x}}(A') + x'\Delta C_p(B) + x'\Delta\mu\frac{dG(\bar{x})}{d\bar{x}}(C)$$

$$+ x'\Delta\rho(D') + u'(E') \tag{23}$$

where constants A', B, C, D', and E' have been defined in Equation (17). Equation (23) can be further simplified into

$$P' = Sx' + E'u' \tag{24}$$

where

$$S = \epsilon\pi DL\Delta t\left[\Delta k\frac{dF(\bar{x})}{d\bar{x}}A' + \Delta C_p B + \Delta\mu\frac{dG(\bar{x})}{d\bar{x}}C + \Delta\rho D'\right]$$

$$E = \epsilon\pi DLE'\Delta t$$

Equation (24) is the general expression which relates the fluctuations in velocity to the fluctions in power and composition. However, one generally measures the root mean square power and then determines the fluctuating velocities. For this purpose Equation (24) may be written as

$$\overline{P'^2} = \overline{S^2 x'^2} + 2\,\overline{SEu'x'} + \overline{E^2 u'^2}$$

$$= \overline{S^2}\;\overline{x'^2} + 2\,\overline{T}\;\overline{u'x'} + \overline{E^2}\;\overline{u'^2} \qquad (25)$$

Thus fluctuating velocity u' can be determined from relation (25) if the three constants appearing in this relation are known. One method of determining these constants would be to calibrate the hot wire at three different temperatures. For further details the reader is referred to an excellent reference by Corrsin (3).

B. Hot Wire Anemometer - Design and Calibration

A hot wire anemometer was designed and constructed so that it might be used to measure time averaged velocities under the conditions of simultaneous mass and momentum transfer as described in Part II. It was calibrated so that it might be used to test applicability of the general equation (Equation(13)) which describes the operation of the hot wire in a gas stream having variable fluid properties. The hot wire probe consists of two sections of stainless steel tubing, 3/8- and 3/16-in. o.d.

as shown in Figure 1. A drawing of the lower half of the probe is shown in Figure 1 A. It is fabricated of a 23-in. long, 3/8-in. o.d. steel tube with a wall thickness of 0.125 in. A male "Sub-Minax" connector is bolted to the top of the tubing. Two pairs of Teflon-coated wires lead from the connector through the tube and are soldered to four terminals of a 5-prong plug attached to the bottom of the probe. The upper section (see Figure 1 B) is fabricated from 3/16-in. o.d. stainless steel tubing (0.018-in. wall thickness). The upper end is bent at an 80° angle so that the wire will be upstream of the main body of the probe, and thus will not sense any distortion caused by the tube.

The probe tip consists of two stainless steel supports cemented to a Bakelite base with Epoxy Resin. The supports are so tapered that the diameter varies from 0.27 in. at the base to 0.015 in. at the tip. Both supports extend 5/8 in. from the surface of the Bakelite housing, and are separated by a distance of 0.125 in. at the base. A 0.00025-in. diameter platinum wire is soldered to the tips of the two prongs. The upper half of the probe is joined to the lower half by a female "Sub-Minax" connector which is cemented to a 1-in. long, 3/16-in. i.d., 1/4-in. o.d. stainless steel collar which in turn fits over the 3/16-in. tubing at its base. Two Teflon-coated wires lead from the two wire supports to the connector at the bottom of this section of the probe.

A Kelvin double-bridge was used to measure the resistance of the platinum wire. The bridge used is similar to that described by Lowell (10).

The hot wire anemometer is calibrated for velocity and temperature in the equipment shown in Figure 2. Compressed air bubbles through

a humidifier, flows through an orifice section where the flow rate is measured, and then through a calming tube where the velocity becomes well developed. The probe is placed at the end of this section. Flow rates are chosen so that the flow is laminar in the tube.

The humidifier is fabricated from a 62-in. length of 2-in. iron pipe. Reducers attached to the ends of this pipe join it to the 1/4-in. brass pipe lines both upstream and downstream of the humidifier. The humidifier is 3/4-filled with 1-in. Berl saddles. Several needle valves upstream and downstream of the humidifier, as well as a pressure regulator facilitate smooth operation of the unit.

The orifice section consists of two lengths of 2-in. i.d. brass tubing (wall thickness = 0.125 in.) and an orifice plate. The upstream section is 30-in. long, has an end-plate soldered to its upstream end and a 3-1/4-in. diameter flange soldered to its downstream end. Radiation Laboratory standard tubing fittings (RL fittings) soldered to the end-plate join the quarter-inch pipe to the orifice section. The downstream section is 20-in. long, and has 3-1/4-in. diameter flanges at both ends. The orifice is fabricated from a 9/32-in. thick sheet of brass. The o.d. is 3-1/4 in., the upstream i.d. is 0.2508 in. The downstream face of the orifice is beveled at a 45° angle to the tube axis as suggested by Stearns et al (20). Two "flange taps" are drilled at locations one-inch upstream and downstream from the face of the orifice plate.

A parabolic laminar velocity profile develops in a 100-in. long, 2-in. i.d. brass calming tube. This section is connected to the orifice

section and probe housing by 3-1/4 in. flanges similar to those used in the orifice section. The probe housing is similar to the calming tube, except that it is only 6-in. long. The probe is inserted at the center-line 2-in. downstream from the first flange. A 20-in. long, 2-in. i.d. brass discharge section is joined to the probe housing by a 3-1/4-in. diameter flange. Heat is supplied to the system by electrical resistance heating tape, which is wrapped around the humidifier walls and the calming tube. The latter is used to keep the wall temperature equal to that of the fluid stream. The power input is controlled by variacs. A manometer manufactured by the Meriam Instrument Co., was used to determine the flow rates through the orifice. The 0.2508-in. diameter orifice was calibrated with a wet test meter.

Before calibration, the wire was visually checked for uniformity of diameter with a 160-power microscope. An increasing amount of current was passed through the wire until it began to become dull red. If the wire diameter was nonuniform, the regions of smallest diameter would become red well before the remainder of the wire due to localized heating. Otherwise, if the wire was uniform, it became dull red at the center first, and a slight increase in current extended the dull-red zone to 80% of the length of the wire. If the wire was acceptable, it was then annealed for approximately two hours by heating it electrically to a dull-red color. It was found, as previously shown by Spangenburg (19) that if this step was not taken, reproducibility in calibration was poor due to hysteresis effects.

The wire was first calibrated for temperature. The probe was inserted in its housing, the calming section heaters turned on, and the air flow set at as high a rate as was possible. An iron-constantan thermocouple was placed very close to the wire. Simultaneous thermocouple emf and wire resistance readings were made at a number of temperatures within the range 20 to 125° C. Wire resistance was plotted as a function of temperature; if the two were related linearly, this served as further evidence that the wire diameter was uniform. Since resistance is a linear function of temperature for the range of 0 to 300° C, the above-mentioned plot was extrapolated to 300° C.

The velocity calibration was also performed in the equipment described above. The humidifier was first filled with water and heated. At the same time, the air was bubbled through the column. The walls of the calibration equipment were also heated. The hot wire anemometer was placed in the housing and attached along with the discharge section to the column section. A gas sampling tube was run in through the discharge section so that the gas stream could be sampled using a thermal conductivity cell as described in detail by Wasan (24).

C. Hot Wire Anemometer - Results and Discussion

General equations (13, 17) which describe the operation of a hot wire anemometer in a gas stream having variable fluid properties have been developed in Section A. In order to illustrate the effect of variable fluid properties on the calibration curve, three hypothetical cases have been computed using Equation (13) for water vapor compositions ranging from 0 to 20 mole percent. The results of these calculations appear in Figure 3. It is noted that in the low velocity range, for a given current and resistance, the velocities at the two extreme compositions differ as much as by 45 percent. It may therefore be concluded that if variation in composition is not accounted for in the interpretation of the experimental data, velocities measured in fields of elevated composition will appear to be higher than the true values.

Data for the velocity calibration performed with air containing 2.29% water vapor and at 22° C are shown in Figure 4 where $\sqrt{u}$ is plotted vs $I^2R_w/\Delta t$. Constants K_1 and K_2 in Equation (13) were determined from the two velocity points shown by the solid points on the figure. The curve corresponding to Equation (13) based on these two points is shown as the upper curve in the figure. It is evident that Equation (13) fits the entire body of velocity data very satisfactorily. It is believed that this constitutes one test of the validity of Equation (13), and thus the satisfactory performance of the hot wire anemometer for measuring the time averaged velocities in a gas mixture. It is to be noted that for velocities greater than 1 ft/sec, the calibration

curve is linear, and Equations (1) and (11) predict the same values. However, at velocities lower than this, the curve is no longer linear and the velocities predicted by King's equation (Equation (1)) are higher than the true values.

Additional calibration data measured in air containing 8.34% water vapor and at 48° C are shown in Figure 5, where these data are compared with the curve corresponding to Equation (11). This curve was computed using the constants K_1 and K_2 that were calculated from data measured in air containing 2.29% water vapor and at 22° C. The satisfactory agreement of the data with the calculated curve demonstrates that once the wire is calibrated at one convenient set of conditions, the resulting constants may be used to calculate velocities measured in a system having different composition and temperature.

As a further test of the performance of the hot wire anemometer, a velocity profile was measured in the calibration equipment where the flow was known to be fully developed and laminar. The measured profile compares well with the anticipated parabolic profile, as may be seen in Figure 6. Since velocities as low as 1 ft/sec were measured, it is believed that this test successfully supports the reliability of the hot wire anemometer at low velocities.

In summary, the results of the present study indicate the applicability of the general equation (Equation (13)) for calculating the time averaged velocities in a field of variable properties. Furthermore, Equation (13) instead of King's equation (Equation (1)) should be used to calculate low velocities. The expression (Equation (17)) has also been developed for calculating the fluctuating velocities. However, the applicability of this equation remains to be tested.

Part
II. MASS AND MOMENTUM TRANSFER STUDIES

Having established confidence in the performance of the hot wire anemometer and the applicability of the general equation as developed in Part I for calculating the time averaged velocities in a field of variable fluid properties, equipment was designed for making the observations of the fully developed turbulent velocity fields in the presence of moderate mass fransfer rates. In the experimental study, water was vaporized from the wetted walls of a short cylindrical section into a fully-developed turbulent air stream. A hot wire anemometer described previously in Part I was used to measure the time-averaged velocity distribution (velocities ranging from 0.2 to 6 feet per second) of the gas stream of variable composition and temperature. Velocity and temperature profiles were measured with and without vaporization conditions for Reynolds numbers ranging from 9,000 to 20,000. This rather narrow range of Reynolds number was chosen because at these flow rates the wall region, where the concentration and velocity gradients are greatest, is relatively large thus facilitating accurate measurements of velocity and concentration in this region.

A. Experimental Apparatus

The equipment shown schematically in Fig. 7 was designed for the study of mass transfer from the liquid to the gaseous phase in mass transfer entry region of a pipe under variable conditions of liquid and gas temperature and Reynolds numbers.

Filtered room air is blown into the apparatus through an orifice meter, an air valve, a bank of nine 0.778 KW finned resistance heaters and a calming section where the velocity profile is allowed to develop before entering the test section.

The air valve and heater are joined to the system by ductwork fabricated of 1/32-in. thick aluminum alloy sheet. The former is joined to the upstream side hose by a duct 23-1/2 in. long, which expands from a 3-1/16-in. outer diameter at the upstream end to a flow area 16 in. by 16 in. at the air valve end. A 1-1/2-in. wide flange is welded around the downstream perimeter so that the duct may be connected to the valve. The air heater is connected in a similar manner to the calming section pipe. The duct upstream flow cross section is 17 in. square, and the downstream inner diameter is 8-5/8 in. This duct is 10 in. long. The air valve is connected to the air heater by a tapered duct fabricated from the same sheet metal as mentioned above. The upstream end has a flow cross section of 16 in. by 16 in., the downstream end cross section is 17 in. square. Both ends have 1-1/2-in. wide flanges welded around their perimeters so that the duct may be attached to the air valve and the heater.

It is desirable that the velocity profile entering the test section be well developed; as a result, a calming section approximately 20 pipe diameters long is used, as recommended by Olsen and Sparrow (14). The calming section is constructed from 7-1/2-in. i.d., 1/4-in. thick aluminum tubing, and is welded to 2 shorter pieces of the same tubing. The 31-3/8-in. length is joined to the air heater exit duct by a sheet of 1/8-in. thick rubber wrapped around the tube and the heater outlet duct lip, and held in place by two 9-in. hose clamps. In

addition, a thermal well is installed in this leg of the section, 8 in. downstream from entry. The temperature sensor inserted in this well is connected to the temperature controller.

The calming section is 168-3/8 in. long. Access to the upstream end of the calming section is provided by a 11-3/8-in. diameter, 1/2-in. thick aluminum end-plate, which is fastened to a flange of the same diameter and thickness on the calming section. Boundary layer growth is initiated by an aluminum ring, 7-1/2-in. o.d., 5/16-in. thick and 1/4-in. deep placed 10-3/4 in. downstream from the flange. The distance from the ring to the head of the test section is 157-3/8 in. which corresponds to an effective calming length of 21 pipe diameters. The downstream end of the tube is joined to the test section by a 1/2-in. thick, 11-3/16-in. diameter aluminum flange. A 3/16-in. diameter pressure tap is drilled 1 in. upstream of the test section entry; 1/4-in. RL fittings are used to provide convenient connection to a pressure gauge. In addition, three traversing ports are provided. The entire calming section, and also the test section are insulated with three layers of fiberglass insulation.

The test section functions as a countercurrent double-pipe mass exchanger. A pictorial view is shown in Fig. 8. Water circulated in the annulus penetrates through the porous pipe and diffuses into the turbulent air stream. The essential component of the test section is a 2-ft long porous ceramic cylinder. An inner diameter of 7.5 in. was chosen so that the concentration boundary layer thickness in the Reynolds number range of interest would be of the order of 0.2 in., thus facilitating concentration measurements at many points within this region. The cylinder is referred to by its manufacturer (Filtros Incorporated) as a "'35' Electrolytic Diaphragm". It is a porous porcelain material of high alumina

content; pore size ranges from 2 to 7.5 microns in radius. The cylinder walls are 7/32 in. thick and will withstand pressures up to 5,000 psig.

Two 11/16-in. diameter holes are drilled 3-1/16 and 15-1/8 in. along the length of the tube to accomodate a probe. These positions shall be referred to as stations I and II respectively. Fifteen iron-constantan thermocouples are installed at stations along the length of the test section. The thermocouples are protected from their wet environment by 3/32-in. o.d. stainless steel tubing (1/16-in. i.d.) and the thermocouple tips are held in place 1/32 in. from the inner surface of the pipe by Saureisen Electrical Cement (no. DW-30). The stainless steel jackets are secured to the outer wall of the ceramic tube by a silicone rubber sealant (GE RTV-102).

The water jacket is fabricated from a 22-3/4-in. length of brass tubing, 10-in. i.d. and 0.148-in. thick. Two 14-in. o.d., 1/2-in. thick brass flanges are welded to the two ends of the tubing. Water enters the annular volume through a 3/4-in. hole drilled 2 in. from the downstream end of the pipe. The water leaves tangentially through a hole of the same diameter drilled 1-3/4 in. from the upstream end of the jacket, and 2-1/16 in. above the center-line, on the left hand side. A hole has also been drilled at the top of the water jacket, 6-5/8 in. downstream from the upstream brass flange to accomodate a pressure gauge and an 18 ft high standpipe which is used both as a test section water pressure indicator and as a vent. Finally, two 3/4-in. holes are drilled as shown to accomodate the probe. When the test section is assembled, the 3/4-in. holes in the jacket are lined up with the holes drilled in the ceramic tube. The probe traversing mechanism is held in place by one of two brass plates, each of which is welded to the outer surface of the jacket, 2-3/4 in. downstream from one of the two probing stations.

The ceramic tube and water jacket are held in place by two 3/4 in. thick, 14-in. diameter aluminum flanges, located at each end of the test section. Seals between the flanges and the ceramic tube and water jacket are obtained by Neoprene O-rings and sealing strips.

Passage to the air stream is provided to the probe by two 3/4-in. o.d. pipes (3/8-in. i.d.), 3-in. long which are inserted in the two 3/4-in. holes drilled at the bottom of the water jacket for that purpose. The uppermost end of the tube rests against a rubber grommet which forms a seal between the ceramic pipe and the tube. Male and female RL fittings are attached to the lower end of the pipe.

The hot wire anemometer probe may be moved through the test section by a traversing mechanism. The gear mechanism is mounted on a 15-7/16-in. by 2-in. by 1/4-in. cold-rolled steel bar. A 3/4-in. pitch diameter spur gear can be moved up and down along a 10-in. long, 32-pitch rack (on the side of the steel bar) by turning the knob mounted on the front of the assembly. Position of the probe is indicated by a scale mounted on the front of the bar, parallel to the probe. The smallest scale division is 1/100th-in.

The discharge section consists of a 7-1/2-in. i.d. (8-in. o.d.), 44-in. length (5-7/8 diameters) of aluminum tubing followed by a 15-in. long, 8-in. square duct. The aluminum tubing is connected to the test section by a 1/2-in. thick, 11-3/16-in. diameter aluminum flange. The square and round ducts are joined by two 10-1/4-in. square flanges (1/8-in. thick). A 3-in. diameter orifice cut in a 10-1/4-in. square sheet of 1/8-in. thick aluminum plate is used to mix the effluent gas stream. The iron duct is then connected to another section of the same cross section by 10-1/4-in. square flanges.

A 2-in. diameter orifice cut in a sheet of aluminum similar to the 3-in. orifice is inserted between the second set of square flanges. A thermometer bulb and gas sampling tube lie in the vena contracta of this orifice, and help to indicate the effluent gas temperature and composition, the latter being measured with a thermal conductivity cell.

Distilled water was stored in a 50-gallon water heater and was filtered and pumped through 1/2-in. copper line and through a rotameter to the test section and then recirculated to the water heater. The temperature of the incoming and outgoing water was noted.

A temperature-compensated aneroid barometer was used to indicate both room and test section total pressure.

B. Experimental Procedure

Velocity profiles were first measured without vaporization. The hot wire anemometer probe was secured at station zero (upstream of the test section), the blower was turned on and the flow rate was set by adjusting the size of the intake port of the blower so that the test section Reynolds number was about 9,500. The center-line velocity and pressure drop across the orifice meter were measured and then rechecked every fifteen minutes until steady values were observed. Then velocity and temperature profiles were measured in the calming section in addition to measurements of air humidity, test section total pressure, pressure drop across orifice meter, orifice meter upstream tap pressure and room temperature. The flow rate was then changed to a Reynolds number of 16,950 and the above procedure was repeated. The procedure for measurement of velocity distributions at stations one and two was identical to that followed at station zero.

Initially, the time averaged velocities were measured along all the radial positions in the test section. Such measurements were made upstream of the test section and at station II which was three pipe diameters downstream of the first profile. All profiles were found to be symmetric about the tube axis and no substantial difference was found between the two profiles taken upstream and downstream of the test section. This would indicate that the velocity profile is well developed.

As a further test of the anemometer and performance of the experimental equipment, Reynolds numbers were computed by averaging the velocity profiles taken at station II without mass transfer. Reynolds numbers of 9,500 and 16,950 were obtained in this manner as compared to 9,240 and 16,500 indicated by the orifice meter readings. The small discrepancy between the two may be attributed to experimental errors associated with the readings of the flow meters used in the anemometer calibration and in the experimental equipment. The close agreement between these two independent methods of estimation of Reynolds numbers indicates that the hot wire anemometer calibration is reliable.

In addition to the above measurements, wire resistance and current were measured in stagnant air across the diameter of the test section to determine the magnitude of the "wall effect" reported by Dryden (5). This effect is caused by the transfer of heat to the pipe wall by natural convection, and leads to velocity readings in the vicinity of the pipe wall which are higher than the true values. For the stagnant air readings mentioned above, it was observed in this study that for the region between the axis of the tube and 0.08 in. from the pipe wall, the heat transferred

from the wire was constant. At distances closer than 0.08 in. from the wall, however, the heat transferred from the wire increased as the wire approached the wall. The amount of heat transferred to the wall was determined by calculating the difference in heat transferred at any point near the wall and the heat transferred at a distance greater than 0.08 in. from the wall. In calculating the true velocity of a gas stream flowing over a heated wire in the vicinity of a solid boundary, it is necessary to subtract the heat transferred to the wall from the total amount of heat transferred from the wire. A wall effect correction curve is given elsewhere (4).

The procedure for the runs performed with mass transfer was similar to that described above with the exception of the operation of the water circulation system. The air flow was set at a rate corresponding to one of the dry runs. Initially, distilled water at room temperature was circulated in the test section annulus at a sufficiently high pressure so that wetting occurred on the inner surface of the ceramic pipe. Once all of the inner surface was visibly wet, the test section water pressure was gradually decreased by reducing the water circulation rate until the rate of penetration of water through the ceramic pipe equaled the rate of diffusion of water into the turbulent air stream. This procedure was checked quantitatively by measuring the composition of the gas stream close to the wall while lowering the test section water pressure. When the walls were wet, the composition of the gas remained constant. For details on the measurement of concentration distribution in the test section, the reader is referred elsewhere (24).

The velocity and temperature profiles were then measured in addition to the test section water pressure, and test section water inlet and outlet temperatures. Velocities were measured at values of the ratio of distance from the pipe wall to the radius (y/r) as small as 0.0045, which corresponds to approximately 100 pipe pore diameters. This distance is believed to be sufficiently large for the wetted surface to appear to be continuous.

B. Experimental Results and Discussion

In order to determine the effects of moderate mass transfer rates on the velocity profile, experimental runs were performed at Reynolds numbers of 9,500 and 16,950 at room temperature conditions and Reynolds number of 9,800 at air and water temperatures of about 50° C. Results of these velocity measurements are shown in Tables 1, 2, and 3. Results of the concentration profiles are given elsewhere (24). Results of the calculated mass transfer rates for the experimental runs are summarized in Table 4. The physical properties of water-vapor air mixture were taken from Reference (7). The log-mean driving force, $(\Delta p_A)_{\ell m}$, was evaluated by using values of the water vapor composition at the test section inlet and at the designated station. The average mass flux, N_A was calculated by a material balance over the corresponding portion of the test section. The mass flux, at the wall, $(N_A)_W$ was calculated by the diffusion equation, and from this value, the ratio of the interfacial

velocity to the maximum velocity, v_W/u_{max} was computed. It is to be noted that the interfacial velocity resulting from the diffusion flux normal to the wall is very much smaller than the minimum point velocity measured in this study.

Velocity profiles measured at room temperature with and without vaporization are compared in Figures 9 and 10. It can be seen from these curves that at low vaporization rates, the velocity distribution remains practically unaltered. In the same manner, velocity profiles measured at 50° C with and without mass transfer are compared in Figure 11. This curve clearly indicates that the mass transfer process does not influence the velocity distribution in any significant way.

Typical concentration profiles measured at Reynolds number of 16,950 are shown in Figure 12. Since concentration gradients are the greatest in the vicinity of the pipe wall, the velocity distribution in this region is of interest. Values of the dimensionless distance, y^+ and dimensionless velocity, u^+ were calculated for the wall region and are compared in Figure 13 with the equations proposed by Wasan, Tien, and Wilke (23) and Von Karman (16). It will be noted that the data from traverses taken both with and without mass transfer agree well with the curves proposed by these authors for the velocity distributions taken without mass transfer, thus indicating that u^+ is a unique function of y^+ under the experimental conditions encountered. It is further noted that velocities were measured at distances as low as about y^+ of 1.0. This indicates the advantage of using a test section of large diameter and low Reynolds range as employed in this study.

A further test of the validity of the experimental data was made by calculating the Fanning friction factors at Reynolds numbers of 9,500, 9,800, and 16,950. Since velocity readings were made at values of y^+ as low as 1.0, it was possible to estimate the velocity gradient at the pipe wall, and thus the shear stress at the wall. The friction factors were then determined using the calculated values of the shear stress at the wall and the bulk velocity of the gas stream. These values compare well with the curve representing the Blasius equation for a smooth pipe, as may be seen in Figure 14. The close agreement observed between calculated and experimental values demonstrates the reliability of hot wire anemometry at the low velocities encountered in this study.

In addition to velocity profiles, the time-averaged temperature distributions corresponding to the velocity profiles were measured at room temperature and Reynolds numbers of 9,500 and 16,950 and at air and water temperatures of about 50° C and Reynolds number of 9,800. The results of the measured temperature profiles are detailed elsewhere (4).

C. Conclusions

In this paper, the hot wire anemometry technique was extended to apply to the measurement of low velocities of gases in a field of variable composition and temperature. Results of the present analysis show that variation in composition and the effects of natural convection must be accounted for in the interpretation of the velocity data. Close agreement between the velocities calculated from Equation (13) and the actual

velocities in known parabolic flow fields established confidence in the hot wire technique for measuring low velocities. Satisfactory performance of the experimental equipment and hot wire anemometer was further substantiated by the fact that Reynolds numbers calculated from the averaged velocity profiles agreed well with those determined from orifice meter readings.

Comparison of velocity profiles measured with and without vaporization indicated that the velocity distributions remained unaffected under the conditions of moderate mass transfer rates. Values of dimensionless distance (y^+) and velocity (u^+) determined from profiles measured with and without vaporization compared well with those calculated from the universal velocity distribution for the wall region proposed by Wasan, Tien, and Wilke. Furthermore, friction factors calculated from the velocity gradients at the pipe wall were in good agreement with those predicted by the Blasius equation.

LITERATURE CITED

1. Cheung, H., L. A. Bromley, and C. R. Wilke, A.I.Ch.E. Journal, 8, p. 221 (1962).

2. Corrsin, S., Rev. Sci. Inst., 18, p. 469 (1947).

3. Corrsin, S., NACA TN 1864 (1949).

4. Davis, R. M., D. T. Wasan, and C. R. Wilke, Lawrence Radiation Laboratory Report UCRL-11552 (1964).

5. Dryden, H. L., NACA Tech. Report No. 562 (1936).

6. Hinze, J. O.,"Turbulence," McGraw-Hill Book Co., Inc., New York (1959).

7. Hov, L. J., University of California Radiation Laboratory Report UCRL-3405 (1959).

8. King, L. V., Phil. Trans. Roy. Soc. (London), Series A 214, p. 373 (1914).

9. King, L. V., Phil. Mag., Series 6, 29, p. 556 (1915).

10. Lowell, H. H., NACA TN 2117 (1950).

11. Merk, H. J., Appl. Sci. Res., A 8, p. 237 (1959).

12. Merk, H. J., Appl. Sci. Res., A 8, p. 261 (1959).

13. Mickley, H. S., R. C. Ross, A. L. Squyers, and W. E. Stewart, NACA TN 3208 (1954).

14. Olsen, R. M., and E. M. Sparrow, A.I.Ch.E. Journal, 9, p. 766 (1963).

15. Reid, R. C., and T. K. Sherwood, "The Properties of Gases and Liquids," McGraw-Hill, New York (1958).

16. Schlichting, H., "Boundary Layer Theory," McGraw-Hill Book Co., New York (1960).

17. Spalding, D. B., Int. J. Heat and Mass Transfer, 2, p. 15 (1961).

18. Spalding, D. B., and H. L. Evans, Int. J. Heat and Mass Transfer, 2, p. 199 (1961).

19. Spangenburg, NACA TN 3381 (1955).

20. Stearns, R. F., R. R. Johnson, R. M. Jackson, and C. A. Larson, "Flow Measurement with Orifice Meters," Van Nostrand Co., Inc., New York (1951).

21. Tewfik, O. E., AIAA Journal, 1, p. 1307 (1963).

22. Van der Hegge Zijnen, B. G., Appl. Sci. Research, 6A, p. 129 (1956).

23. Wasan, D. T., C. L. Tien, and C. R. Wilke, A.I.Ch.E. Journal, 9, p. 567 (1963).

24. Wasan, D. T., and C. R. Wilke, Lawrence Radiation Laboratory Report UCRL-11629, September 1964.

ACKNOWLEDGMENT

This work was done under the auspices of the U. S. Atomic Energy Commission.

NOTATION

a	constant appearing in King's equation (Equation (1))	
A	surface area of a cylinder available for heat transfer	(ft^2)
b	constant appearing in King's equation (Equation (1))	
C_p	specific heat	(Btu/hr $^\circ$ F)
D	diameter	(ft)
f	Fanning friction factor	
g	acceleration due to gravity	(lb./ft^2)
h	heat transfer coefficient	$\frac{\text{ft.-lb.}}{\text{lb.-force sec}}$
I	electrical current flowing through wire	(mA)
k	thermal conductivity	(Btu/hr ft $^\circ$ F)
K_1, K_2	constants appearing in Equation (13)	
L	length of wire	(ft)
N_A	mass flux of diffusing species	(g.moles/cm^2sec)
P_A	vapor pressure of diffusing species	(mm. Hg)
r	pipe radius	(ft)
R	wire resistance	(ohms)
t	temperature	($^\circ$ F or $^\circ$C)
u	fluid velocity	(ft/sec)
u_τ	friction velocity = $\sqrt{\tau_W g_c/\rho}$	(ft/sec)
v	radial velocity	(ft/sec)
y	distance from pipe wall	(ft)

NOTATION (Cont'd)

Greek Letters

β'	coefficient of expansion of gas	
ϵ	energy conversion factor	(μW-hr/Btu)
κ	orifice discharge coefficient	
μ	fluid viscosity	(lb./ft hr)
ν	kinematic viscosity	(ft^2/hr)
ρ	fluid density	(lb./ft^3)

Dimensionless Groups

Gr	Grashof number	$(g\rho^2 D^3 \beta' \Delta t/\mu^2)$
Nu	Nusselt number	(hD/k)
Pr	Prandtl number	$(C_p \mu/k)$
Re	Reynolds number	$(Du\rho/\mu)$
u^+	dimensionless velocity	(u/u_τ)
y^+	dimensionless distance	(yu_τ/ν)

Subscripts

a	air
f	mean (arithmetic) film
fo	forced convection
i	inlet
ℓm	log mean
max	maximum
n	natural convection
r	radiation
t	total of natural, forced convection and radiation
w	wire
W	wall

Table 1. Tabulated velocity profiles measured at a Reynolds number of 9,500 and an approximate air temperature of 25° C.

Station I (z/d=.216)				Station II (z/d=1.82)			
Dry run		Mass transfer run		dry run		Mass transfer run	
y/r	u/u_{max}	y/r	u/u_{max}	y/r	u/u_{max}	y/r	u/u_{max}
0.0104	0.134	0.0109	0.155	0.0045	0.070	0.0051	0.085
0.0163	0.268	0.0163	0.246	0.0099	0.139	0.0104	0.144
0.0243	0.362	0.0243	0.357	0.0179	0.268	0.0184	0.288
0.0376	0.516	0.0376	0.531	0.0312	0.441	0.0317	0.468
0.0509	0.613	0.0509	0.603	0.0445	0.556	0.0451	0.546
0.0643	0.670	0.0643	0.679	0.0579	0.632	0.0584	0.626
0.0776	0.721	0.0776	0.712	0.0712	0.705	0.0717	0.688
0.1043	0.765	0.1043	0.784	0.0979	0.752	0.0984	0.755
0.1576	0.842	0.1576	0.839	0.1512	0.836	0.1517	0.796
0.2909	0.885	0.2909	0.874	0.2845	0.881	0.2851	0.875
0.4243	0.914	0.4243	0.942	0.4179	0.915	0.4184	0.930
0.5576	0.963	0.5576	0.961	0.5512	0.947	0.5517	0.951
0.6909	0.974	0.6909	0.976	0.6845	0.971	0.6851	0.964
0.8243	0.995	0.8243	0.981	0.8179	0.989	0.8184	0.986
0.9576	0.995	0.9576	1.000	0.9512	0.989	0.9517	0.986

Maximum velocity = u_{max} = 3.143 ft/sec

Table 2. Tabulated velocity profiles measured at a Reynolds number of 16,950 and an approximate air temperature of 25° C.

Station I (z/d=.216)				Station II (z/d=1.82)			
Dry run		Mass transfer run		Dry run		Mass transfer run	
y/r	u/u_{max}	y/r	u/u_{max}	y/r	u/u_{max}	y/r	u/u_{max}
0.0104	0.274	0.0109	0.198	0.0045	0.120	0.0051	0.162
0.0163	0.390	0.0163	0.372	0.0099	0.223	0.0104	0.235
0.0243	0.531	0.0243	0.490	0.0179	0.405	0.0184	0.436
0.0736	0.657	0.0376	0.636	0.0312	0.603	0.0317	0.639
0.0509	0.732	0.0509	0.721	0.0445	0.699	0.0451	0.685
0.0643	0.748	0.0643	0.742	0.0579	0.726	0.0584	0.720
0.0776	0.777	0.0776	0.762	0.0712	0.757	0.0717	0.750
0.1043	0.810	0.1043	0.803	0.0979	0.818	0.0984	0.802
0.1576	0.842	0.1576	0.831	0.1512	0.849	0.1517	0.840
0.2909	0.885	0.2909	0.887	0.2845	0.896	0.2851	0.925
0.4243	0.914	0.4243	0.938	0.4179	0.931	0.4184	0.935
0.5576	0.963	0.5576	0.959	0.5512	0.975	0.5517	0.980
0.6909	0.974	0.6909	0.972	0.6845	0.990	0.6851	0.991
0.8243	0.995	0.8243	0.982	0.8179	0.995	0.8184	0.999
0.9576	0.995	0.9576	0.986	0.9512	1.000	0.9517	0.999

Maximum velocity = u_{max} = 5.355 ft/sec

Table 3. Tabulated velocity profiles measured at a Reynolds number of 9,800 and an approximate air temperature of 50° C.

y/r	Dry run u/u_{max}	Mass transfer run u/u_{max}
0.0069	0.113	0.155
0.0123	0.191	0.194
0.0203	0.310	0.320
0.0336	0.518	0.496
0.0469	0.654	0.629
0.0603	0.702	0.688
0.0736	0.795	0.744
0.1003	0.839	0.827
0.1536	0.895	0.878
0.2869	0.956	0.931
0.4203	0.983	0.960
0.5536	0.998	0.977
0.6869	1.000	0.977
0.9536	0.998	0.972

Maximum velocity = u_{max} = 3.611 ft/sec

Table 4. Summary of calculated mass transfer rates.

Run no.	Station no.	Reynolds no. Re	Log-mean[a] driving force (mm. Hg) $\Delta P_{\ell m}$	Average[a] mass flux (g.moles/cm^{2}sec × 10^6) N_A	Mass flux at the wall N_{A_W}	$v_W/u_{max} \times 10^4$
W-2	I	9,500	12.42	1.985	1.285	3.39
W-2	II	9,500	12.16	0.521	0.430	1.14
W-3	I	16,950	10.61	1.060	0.960	1.49
W-3	II	16,950	10.42	0.442	0.351	0.54
W-4	II	9,800	70.51	5.220	2.120	5.24

[a]Average taken between test section inlet and corresponding station.

Figure Captions

Fig. 1. Engineering drawings of how wire anemometer probe.

(a) Lower half. (b) Upper half.

Fig. 2. Equipment used for calibration of hot wire anemometer.

Fig. 3. Effect of water vapor on hot wire anemometer calibration curve for air according to Equation (13). Wire diameter = 0.00025 in; wire length = 0.10 in; wire mean film temperature = 152° C.

Fig. 4. Comparison of velocity calibration data measured in air with water vapor composition of 2.29% at 22° C with Equations (1) and (13).

Fig. 5. Comparison of velocity calibration data measured in air containing 8.34% water vapor and at 48° C with Equation (13).

Fig. 6. Velocity profile in hot wire anemometer calibration equipment.

Fig. 7. Schematic of mass and momentum transfer equipment.

Fig. 8. Pictorial view of test section.

Fig. 9. Comparison of velocity profiles measured with and without mass transfer at about 25° C and Reynolds number of 9,500 (u_{max} = 3.143 ft/sec).

Fig. 10. Comparison of velocity profiles measured with and without mass transfer at about 25° C and Reynolds number of 16,950 (u_{max} = 5.355 ft/sec).

Fig. 11. Comparison of velocity profiles measured with and without mass transfer at 50° C and a Reynolds number of 9,800 (u_{max} = 3.611 ft/sec).

Fig. 12. Concentration profiles in the test section at a Reynolds number of 16,950.

Fig. 13. Comparison of experimental data measured near the pipe wall with known velocity distributions for turbulent flow in a pipe.

Fig. 14. Fluid friction in experimental apparatus.

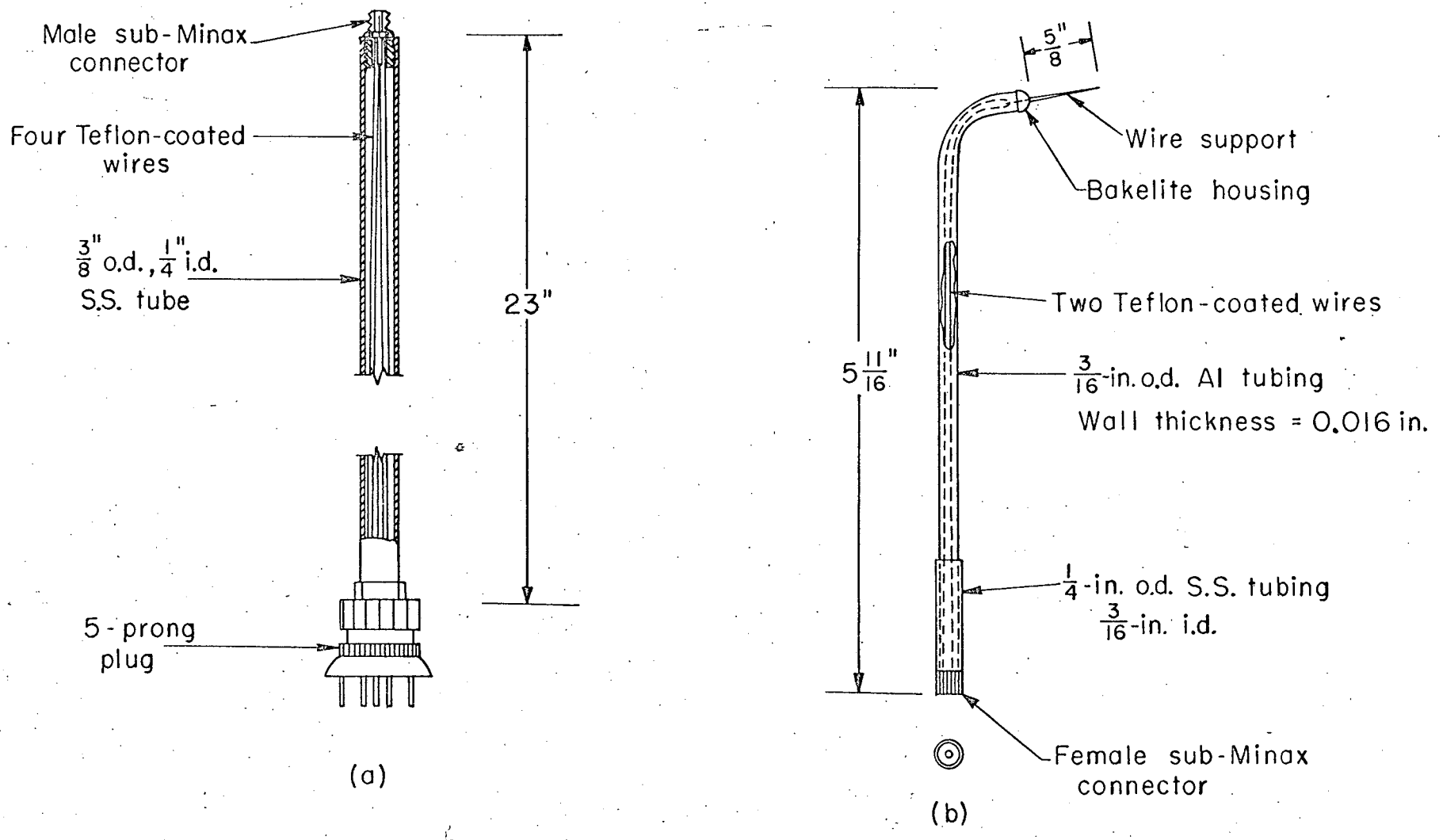

Fig. 1

MU-34420

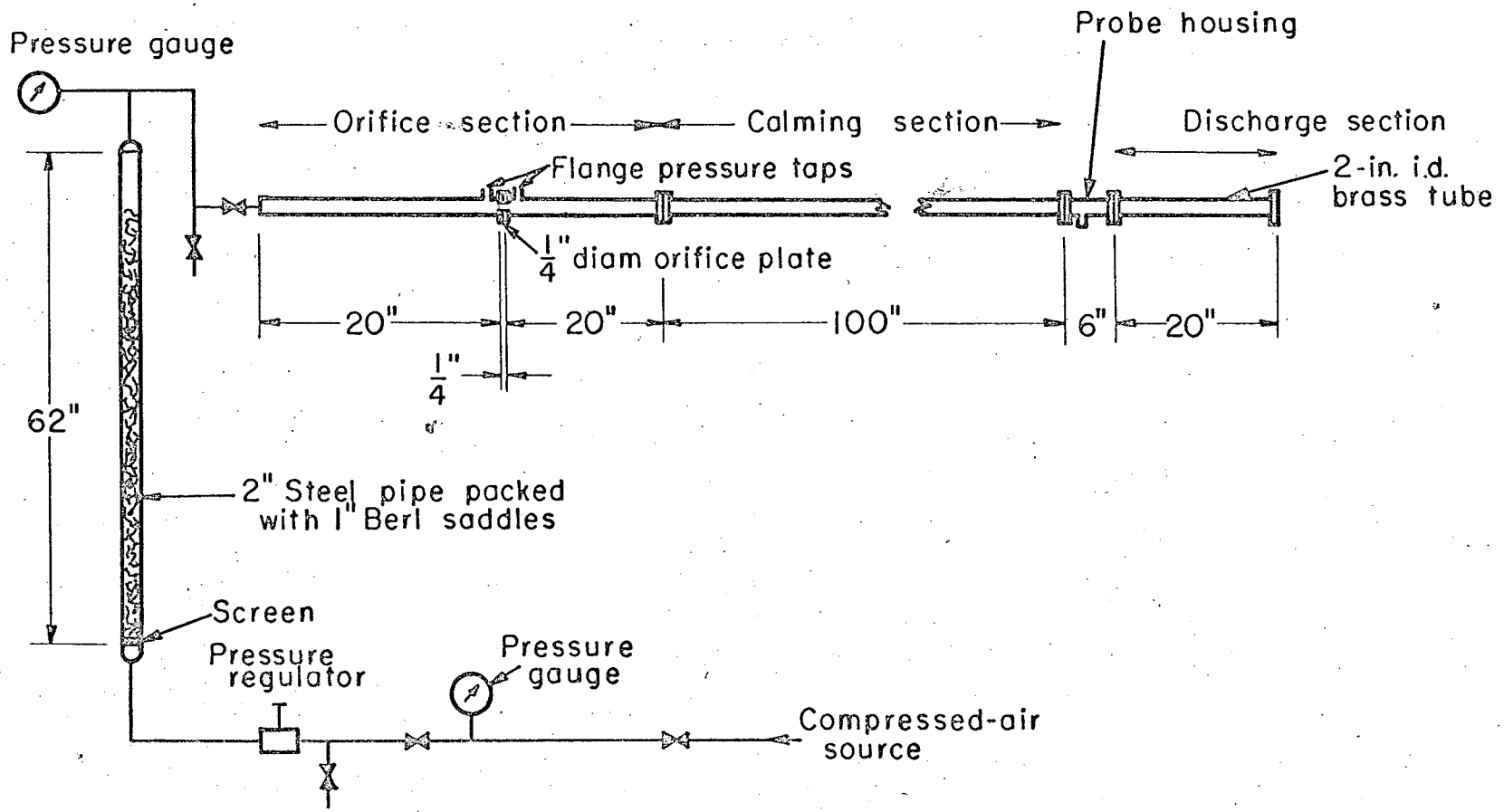

Fig. 2

MU-34426

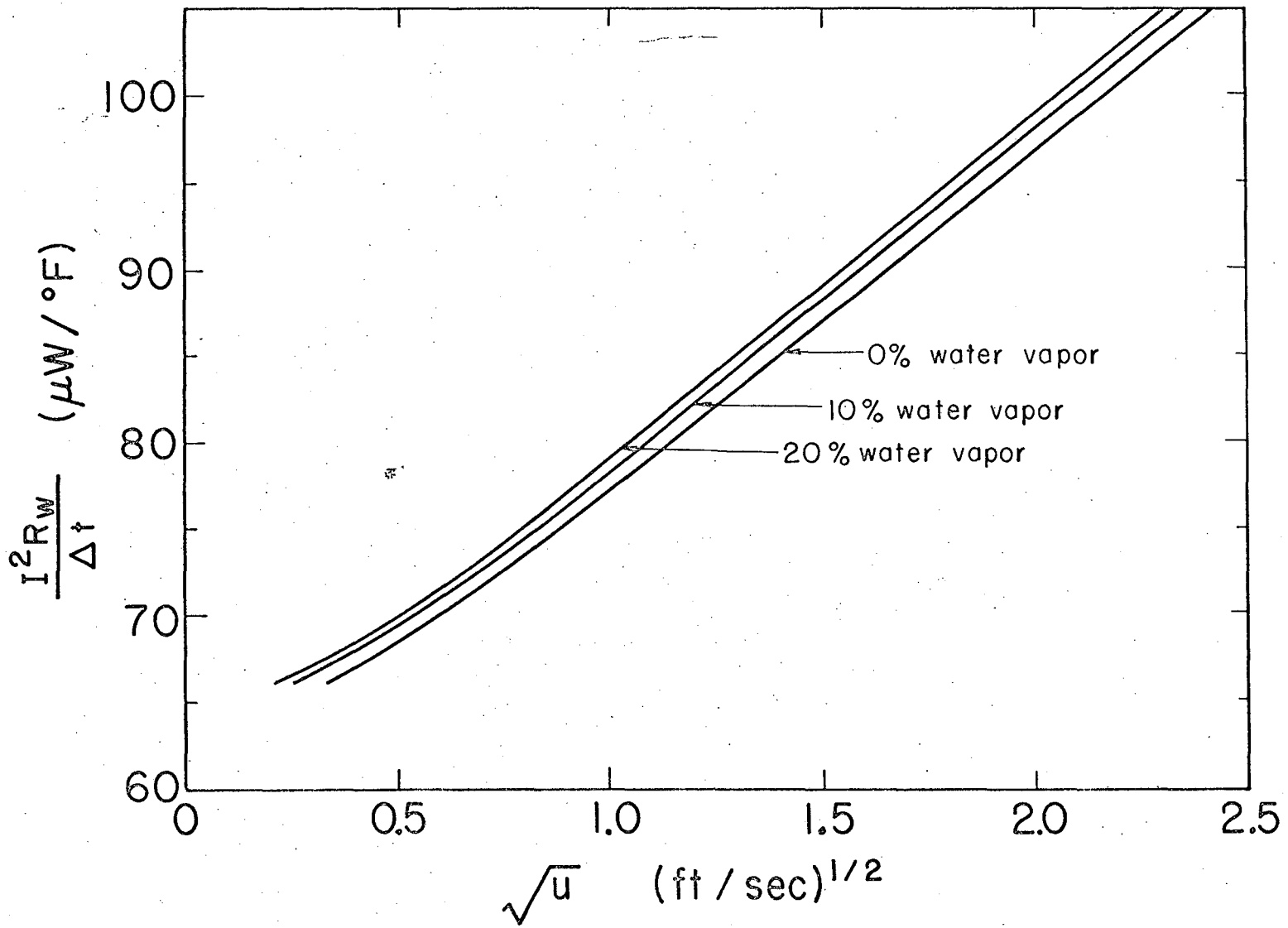

Fig. 3

MU-34567

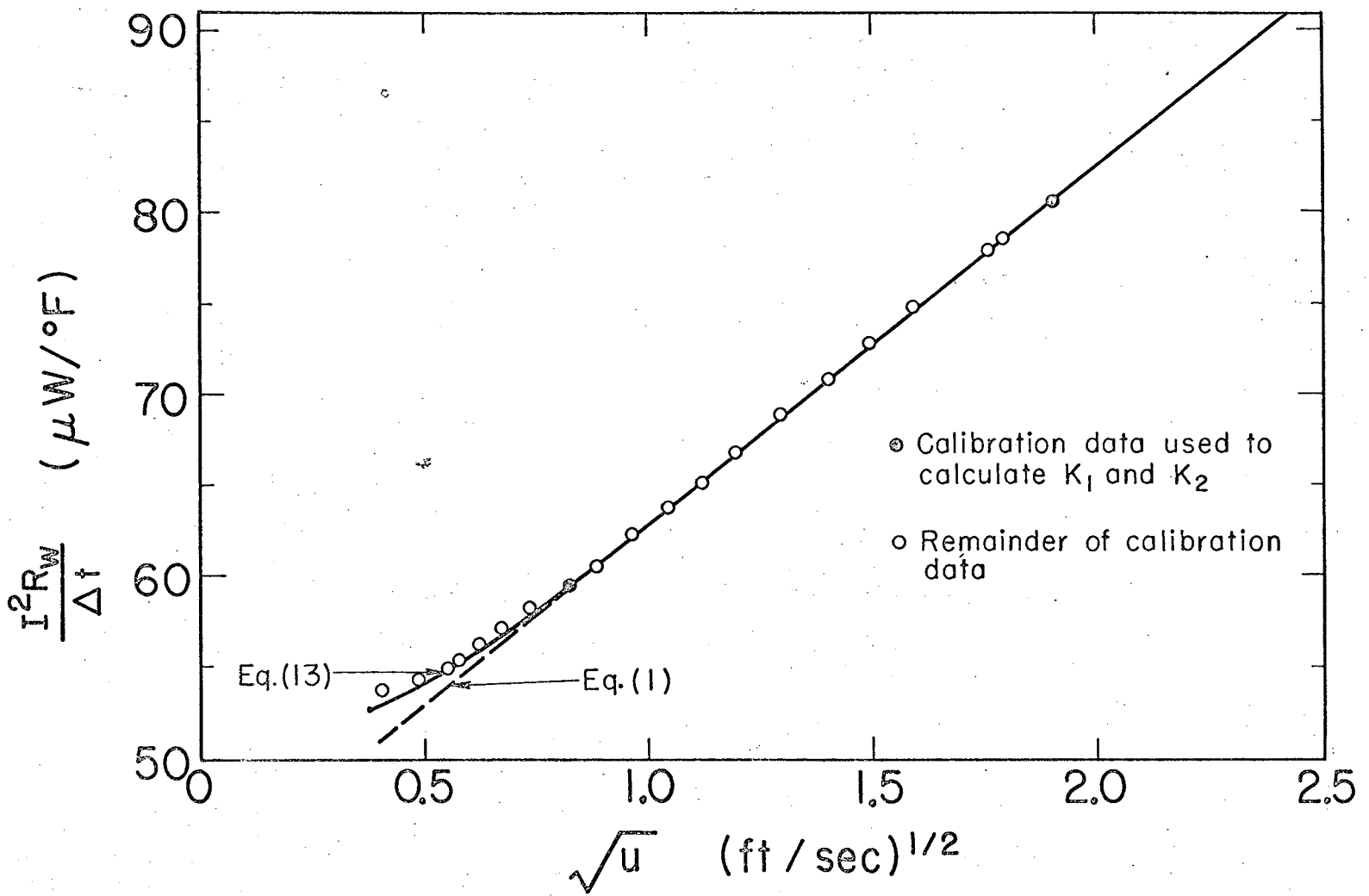

MU-34568

Fig. 4

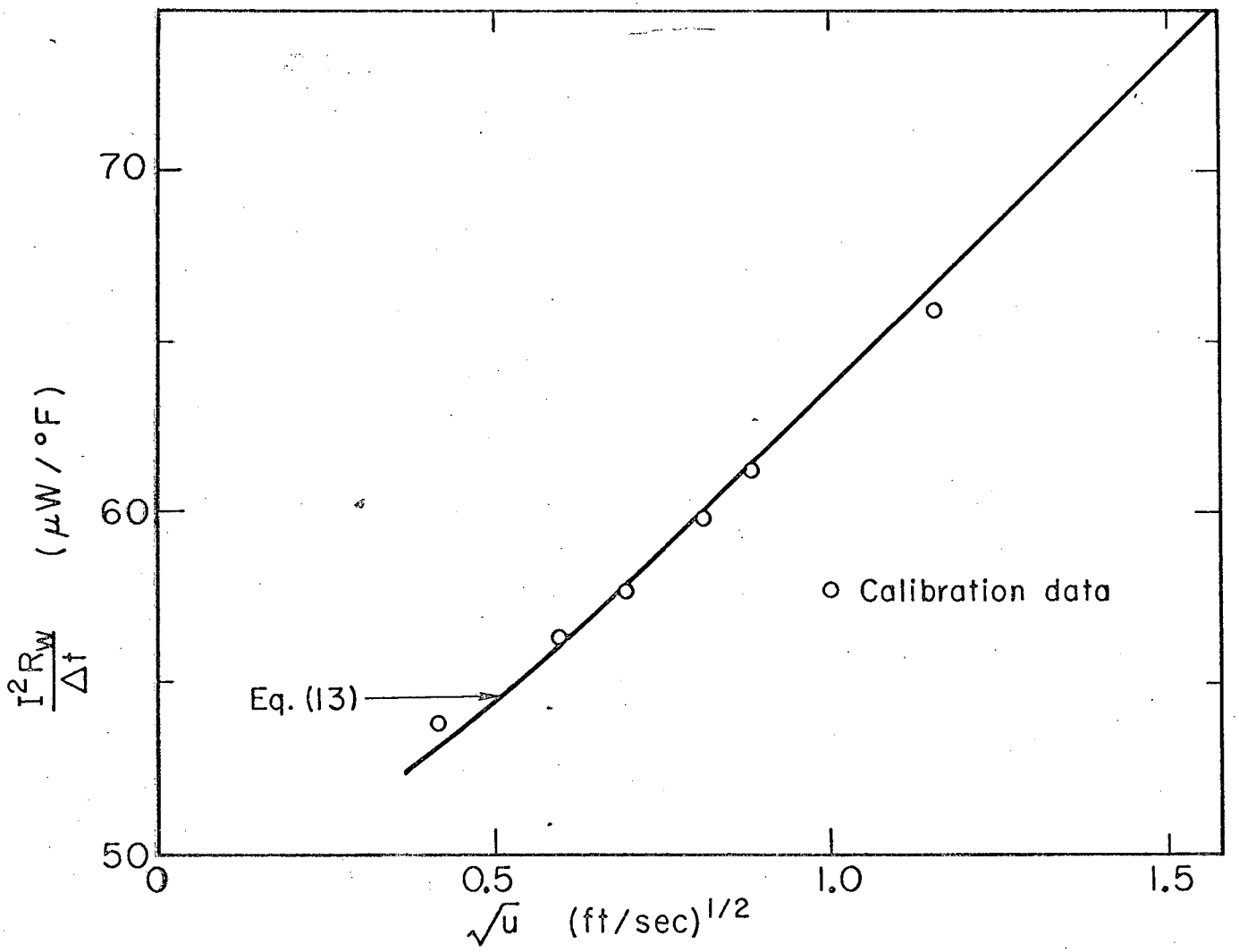

Fig. 5

MU-34569

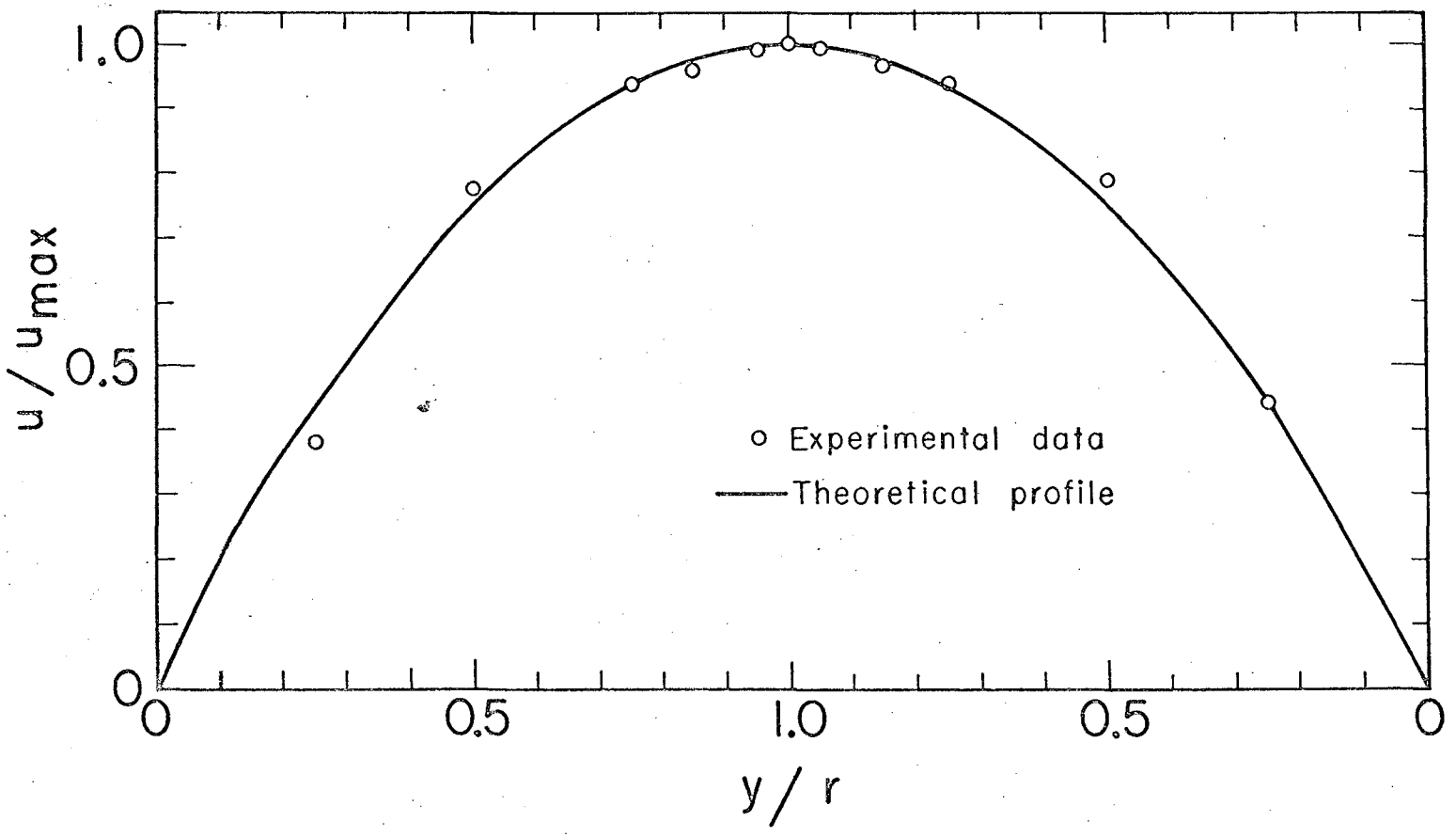

MU-34411

Fig. 6

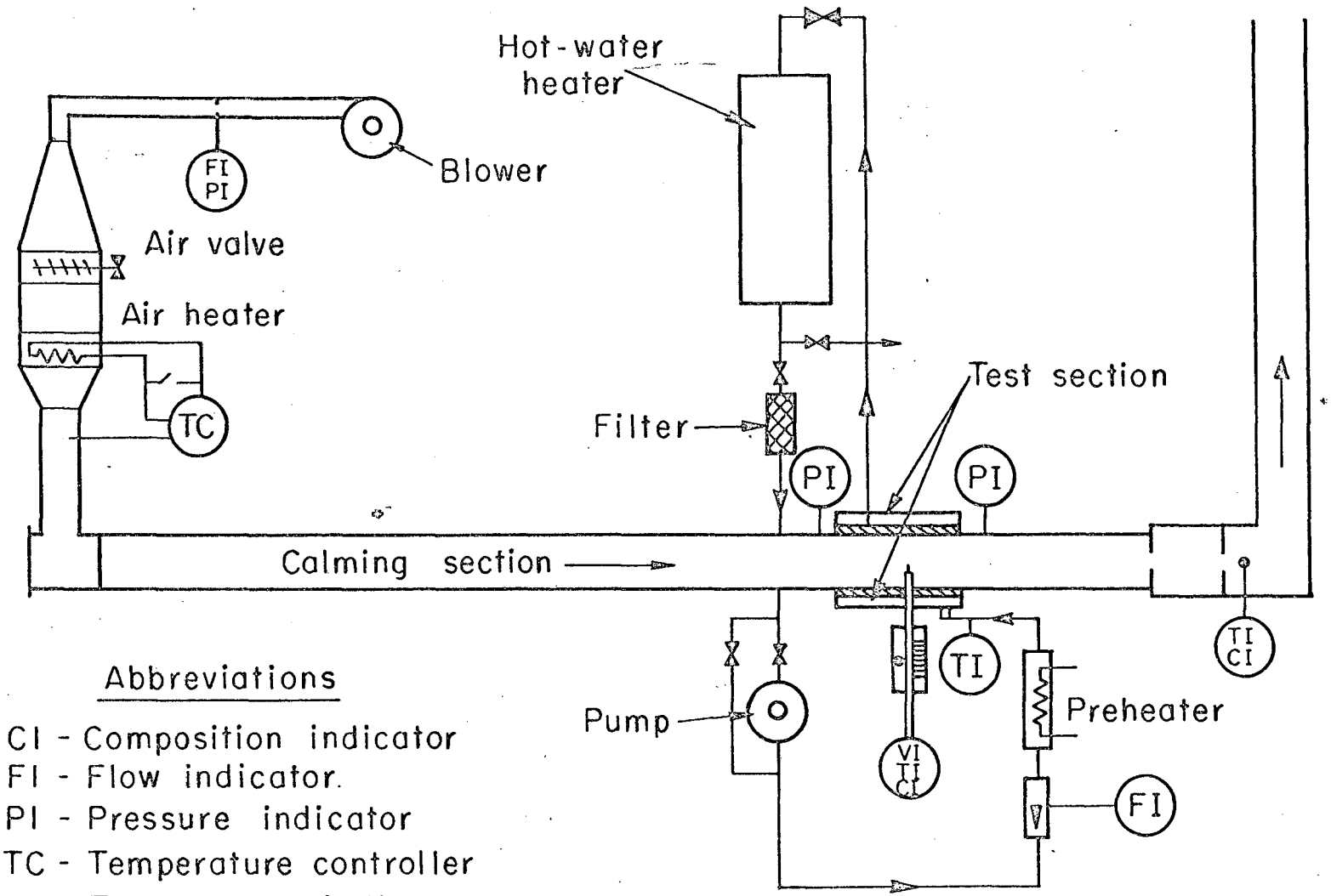

Abbreviations

CI - Composition indicator
FI - Flow indicator.
PI - Pressure indicator
TC - Temperature controller
TI - Temperature indicator
VI - Velocity indicator

MU-34422

Fig. 7

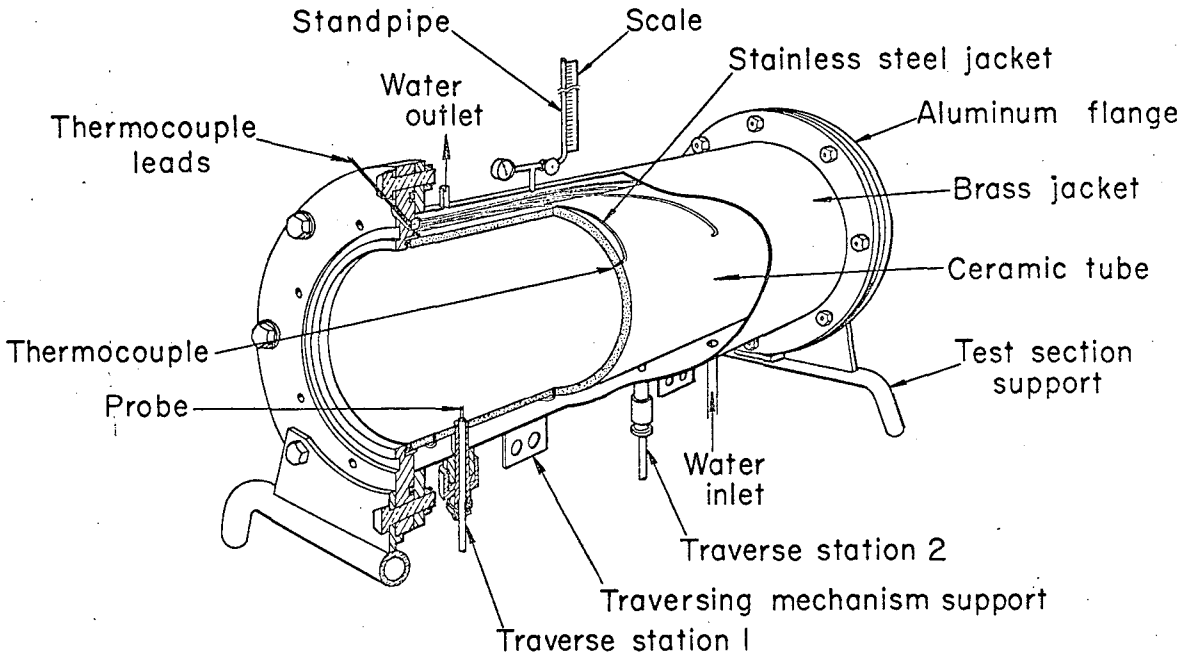
Standpipe
Scale
Stainless steel jacket
Water outlet
Thermocouple leads
Aluminum flange
Brass jacket
Ceramic tube
Thermocouple
Probe
Test section support
Water inlet
Traverse station 2
Traversing mechanism support
Traverse station I
MUB-2516

Fig. 8

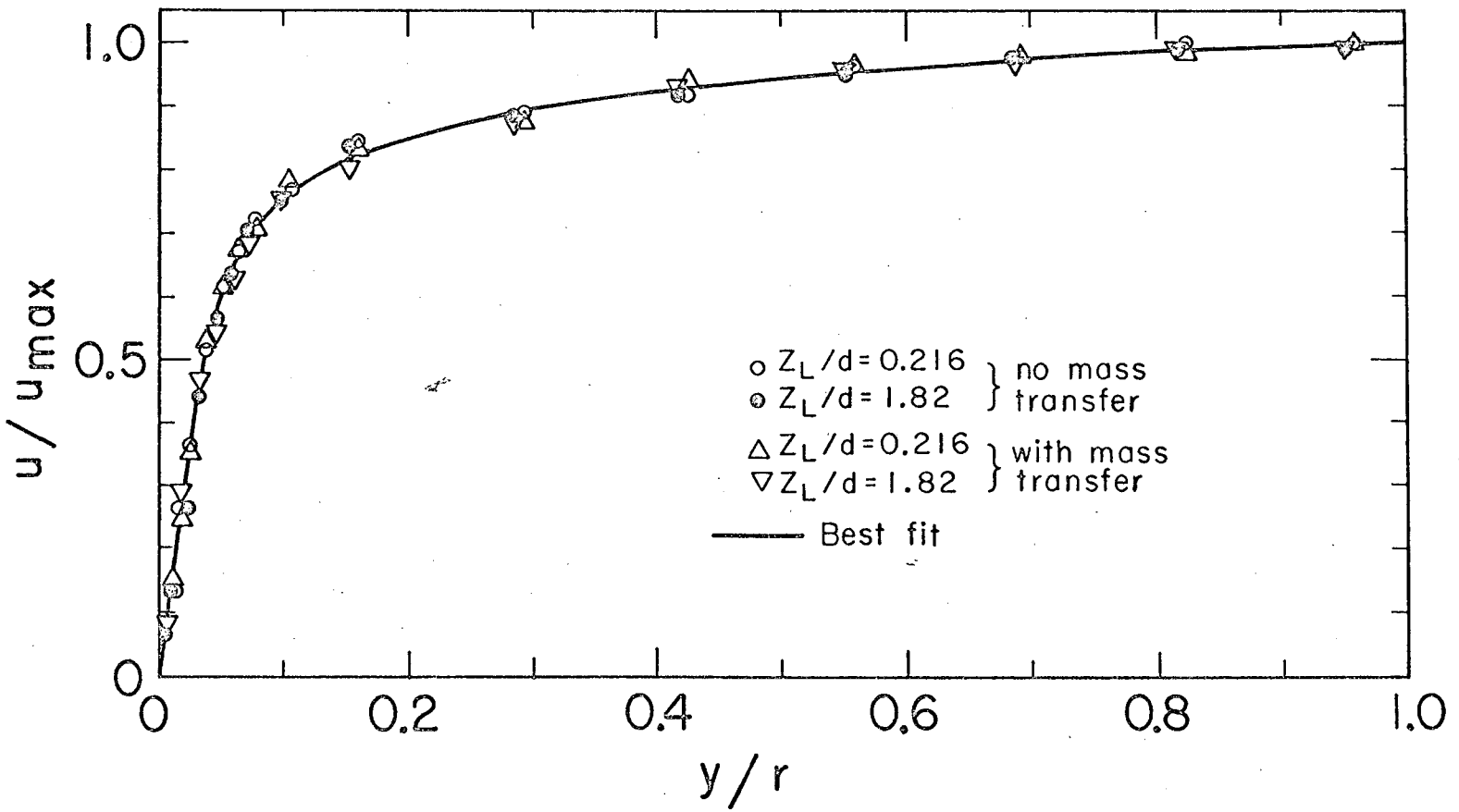

MU-34410

Fig. 9

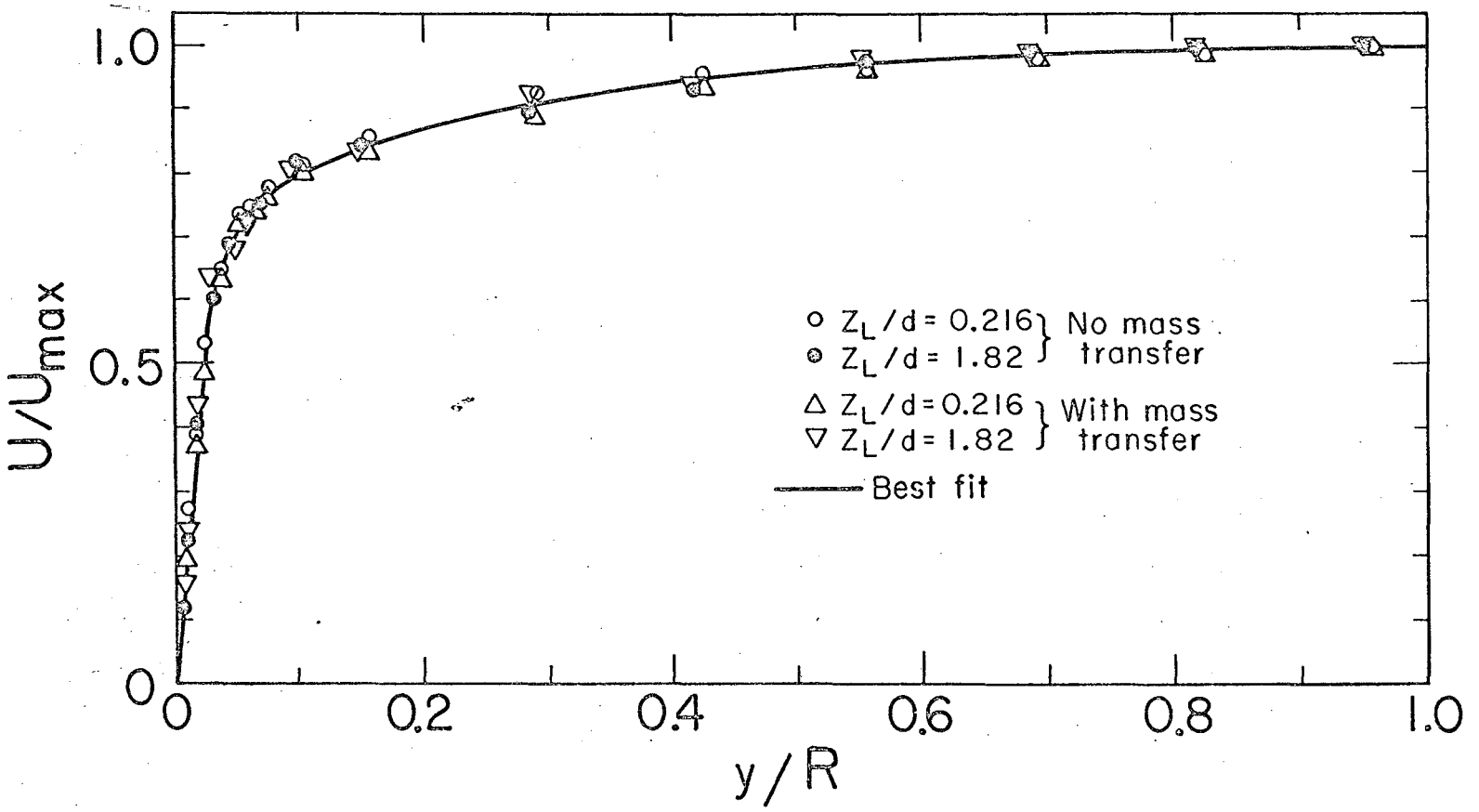

MU-34408

Fig. 10

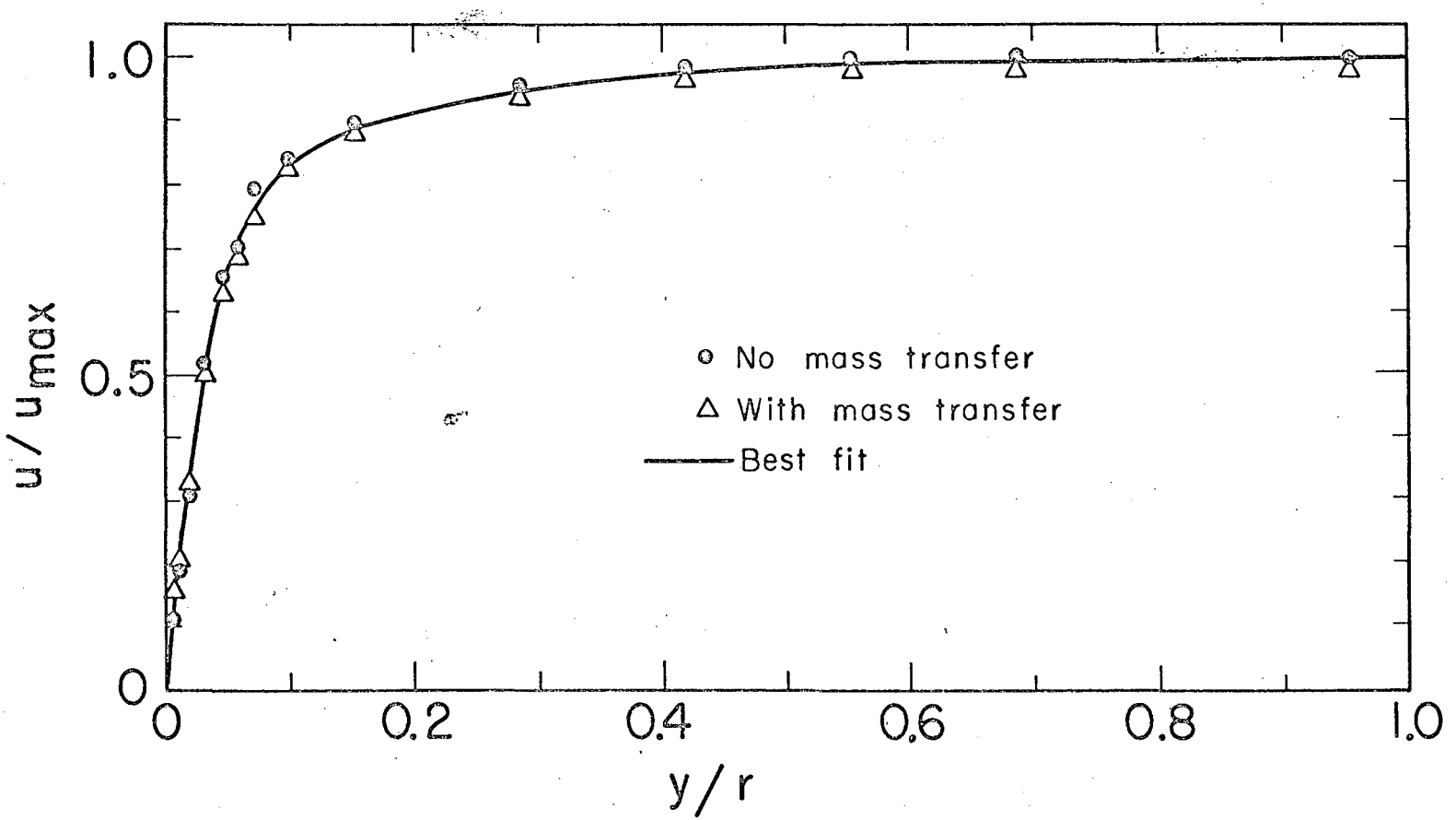

MU-34407

Fig. 11

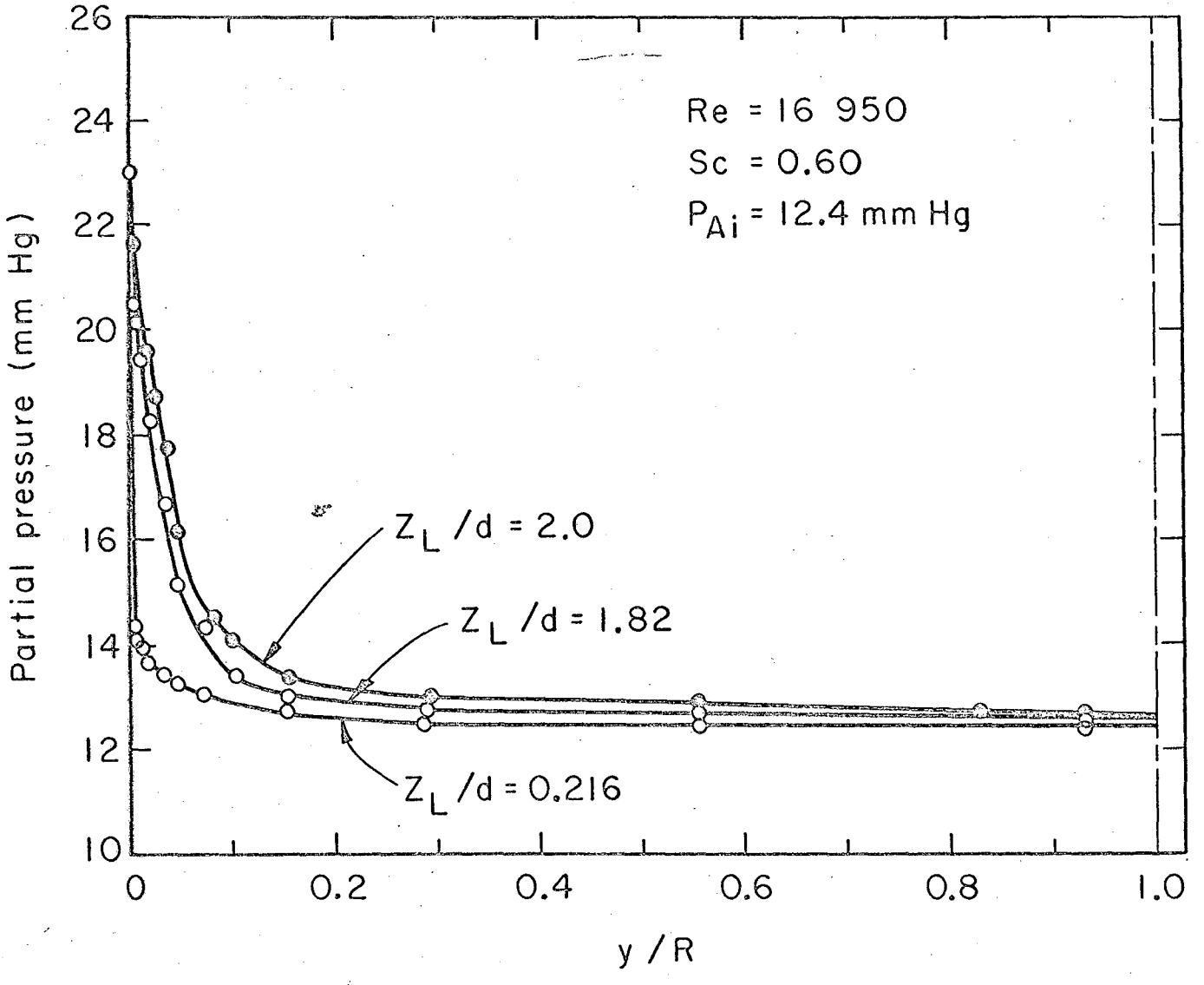

Fig. 12

MU-34762

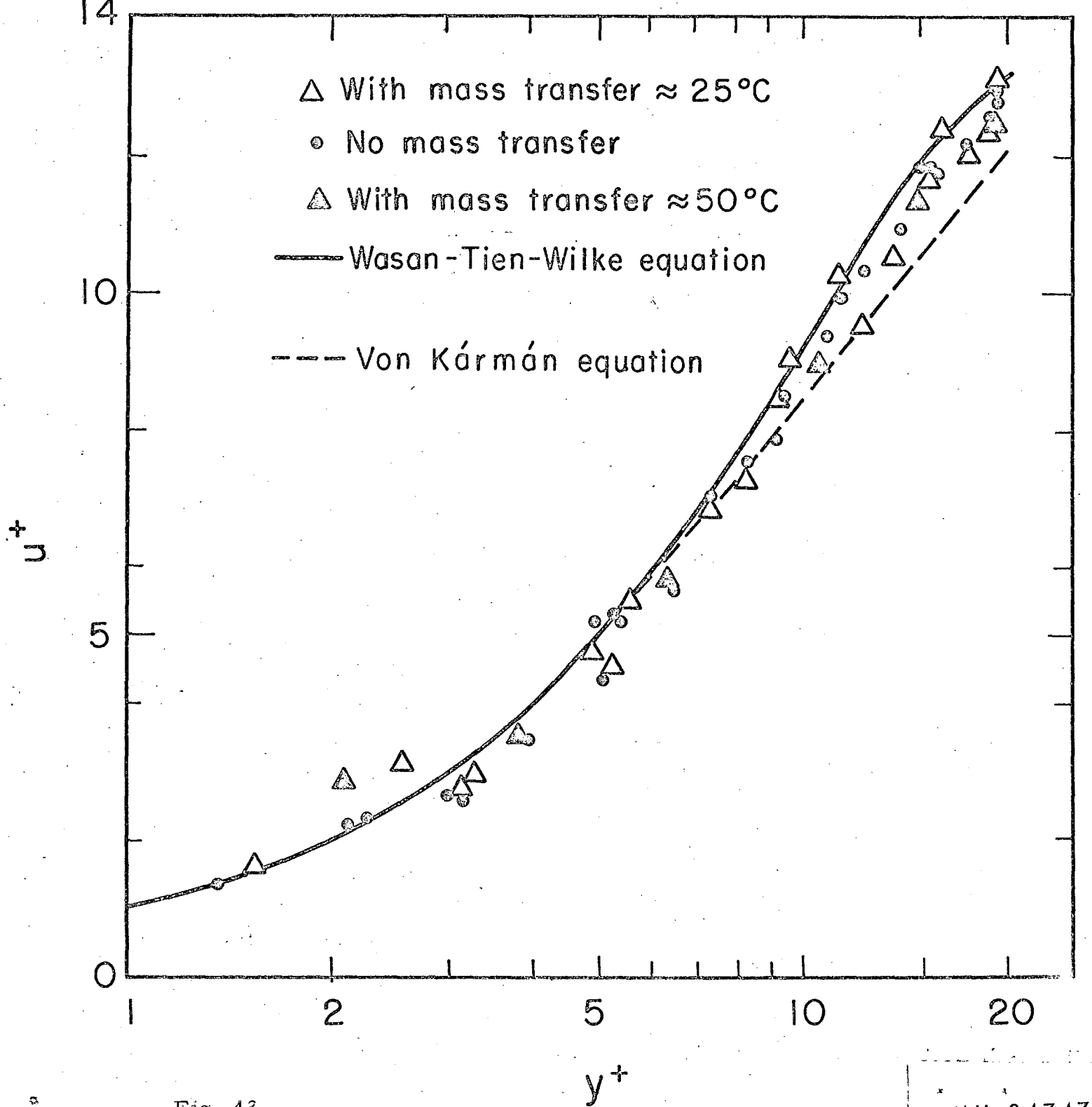

Fig. 13

MU-34747

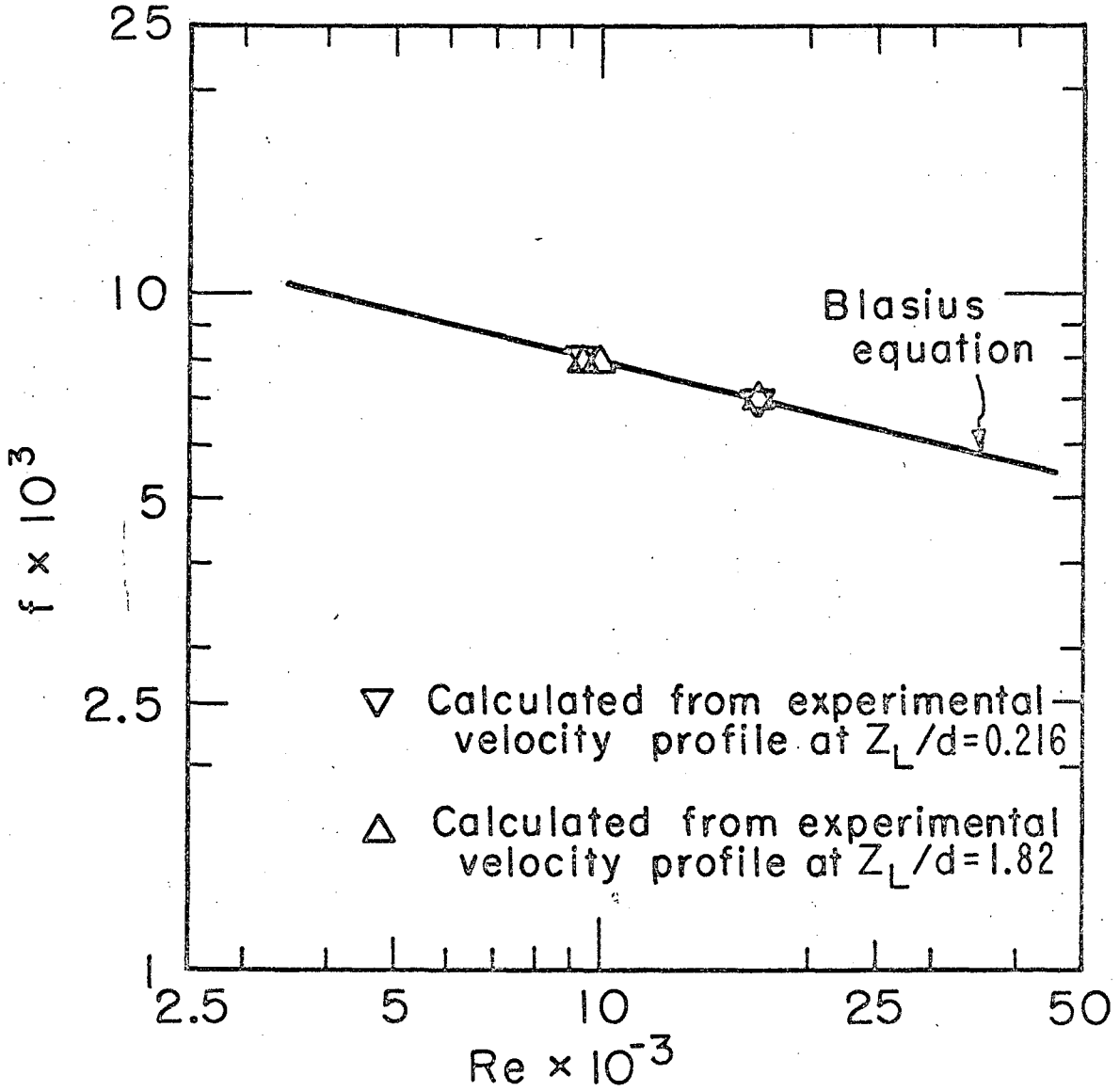

MU-34403

Fig. 14

This report was prepared as an account of Government sponsored work. Neither the United States, nor the Commission, nor any person acting on behalf of the Commission:

A. Makes any warranty or representation, expressed or implied, with respect to the accuracy, completeness, or usefulness of the information contained in this report, or that the use of any information, apparatus, method, or process disclosed in this report may not infringe privately owned rights; or

B. Assumes any liabilities with respect to the use of, or for damages resulting from the use of any information, apparatus, method, or process disclosed in this report.

As used in the above, "person acting on behalf of the Commission" includes any employee or contractor of the Commission, or employee of such contractor, to the extent that such employee or contractor of the Commission, or employee of such contractor prepares, disseminates, or provides access to, any information pursuant to his employment or contract with the Commission, or his employment with such contractor.